

# Cool White Dwarfs in the Sloan Digital Sky Survey<sup>1,2</sup>

Mukremin Kilic<sup>3,7</sup>, Jeffrey A. Munn<sup>4</sup>, Hugh C. Harris<sup>4</sup>, James Liebert<sup>5</sup>, Ted von Hippel<sup>3</sup>,  
Kurtis A. Williams<sup>5</sup>, Travis S. Metcalfe<sup>6</sup>, D. E. Winget<sup>3</sup>, and Stephen E. Levine<sup>4</sup>

## ABSTRACT

A reduced proper motion diagram utilizing Sloan Digital Sky Survey (SDSS) photometry and astrometry and USNO-B plate astrometry is used to separate cool white dwarf candidates from metal-weak, high-velocity main sequence Population II stars (subdwarfs) in the SDSS Data Release 2 imaging area. Follow-up spectroscopy using the Hobby-Eberly Telescope, the MMT, and the McDonald 2.7m Telescope is used to demonstrate that the white dwarf and subdwarf loci separate cleanly in the reduced proper motion diagram, and that the contamination by subdwarfs is small near the cool white dwarf locus. This enables large statistically complete samples of white dwarfs, particularly the poorly understood cool white dwarfs, to be created from the SDSS imaging survey, with important implications for white dwarf luminosity function studies. SDSS photometry for our sample of cool white dwarfs is compared to current white dwarf models.

*Subject headings:* stars: atmospheres—stars: evolution—white dwarfs

---

<sup>1</sup>Based on observations obtained with the Hobby-Eberly Telescope, which is a joint project of the University of Texas at Austin, the Pennsylvania State University, Stanford University, Ludwig-Maximilians-Universität München, and Georg-August-Universität Göttingen.

<sup>2</sup>Observations reported here were obtained at the MMT Observatory, a joint facility of the Smithsonian Institution and the University of Arizona.

<sup>3</sup>The University of Texas at Austin, Department of Astronomy, 1 University Station C1400, Austin, TX 78712

<sup>4</sup>US Naval Observatory, P.O. Box 1149, Flagstaff, AZ 86002

<sup>5</sup>Steward Observatory, University of Arizona, 933 North Cherry Avenue, Tucson, AZ 85721

<sup>6</sup>Harvard-Smithsonian Center for Astrophysics, Mail Stop 16, 60 Garden Street, Cambridge, MA 02138

<sup>7</sup>kilic@astro.as.utexas.edu

## 1. Introduction

The white dwarf luminosity function of the Galactic disk has traditionally been used as one tool to estimate the star formation history and age of this population (Liebert 1979; Winget et al. 1987; Liebert, Dahn & Monet 1988). The largest samples to date used to determine the white dwarf luminosity function are those of Fleming et al. (1986; see Liebert, Bergeron & Holberg 2004 for an updated version) on the hot end and Oswalt et al. (1996, using white dwarfs in common proper motion binaries) on the cool end. The most commonly used luminosity function for cool white dwarfs (Liebert, Dahn, & Monet 1988) was based on a sample of only 43 stars selected on the basis of large proper motion from the Luyten Half Second Proper Motion Survey (Luyten 1979). Questions about completeness and kinematic selection bias have been raised over the years, and the need to construct a larger, deeper and more complete sample has been obvious. Of even greater interest is the possibility of delineating a useful sample of white dwarfs from the local halo, which may be drawn largely from a single burst of star formation at a greater age than the disk. Oppenheimer et al. (2001) claimed to have found a significant population of halo white dwarfs from kinematic surveys, though these claims were later disputed by several investigators (Reid et al. 2001; Reyle et al. 2001; Silvestri, Oswalt, & Hawley 2002; Bergeron 2003; Spagna et al. 2004).

The Sloan Digital Sky Survey (SDSS, York et al. 2000) offers a valuable new resource which may be used to identify a significantly larger white dwarf sample. Imaging is performed in five broad optical bands ( $u$ ,  $g$ ,  $r$ ,  $i$ , and  $z$ ) down to  $\sim 22$  magnitude in  $u$ ,  $g$ , and  $r$  with 95% completeness for point sources. Hot white dwarfs can be identified efficiently due to their blue colors (Fan 1999; Kleinman et al. 2004), but white dwarfs near or below the temperatures of Population II main sequence turnoff stars are buried in the stellar locus. Methods such as the use of an intermediate-band filter to find stars with no MgH absorption feature (Claver 1995) turned out to be less efficient than expected (Kilic et al. 2004). However, the reduced proper motion technique (Luyten 1918) offers an efficient means to identify cooler white dwarfs, as well as halo white dwarfs, by their underluminosity in comparison to main sequence stars with similar colors, and their high space motions.

An improved proper-motion catalog combining the USNO-B (Monet et al. 2003; 5 epochs) and SDSS catalogs in the area of sky covered by SDSS Data Release 1 (DR1; Abazajian et al. 2003) is presented by Munn et al. (2004). They used SDSS astrometry to recalibrate the USNO-B plate astrometry, reducing both the statistical and systematic errors significantly. In addition, SDSS positions were used to eliminate the large number of false high proper motion objects in the USNO-B catalog.

The combination of accurate SDSS photometry and SDSS+USNO-B astrometry enables us to construct a reduced proper motion diagram and select cool white dwarf candidates

from the disk and halo. This paper presents results from the first year of our spectroscopic campaign. In §2 we present the reduced proper motion diagram from SDSS Data Release 2 and review our target selection criteria for follow-up spectroscopy. Our spectroscopic observations are described in §3, while an analysis of the observational material and results from this analysis is presented in §4. Various implications of these results are then discussed in §5.

## 2. Target Selection

The reduced proper motion, defined as  $H = m + 5 \log \mu + 5$ , where  $m$  is the apparent magnitude and  $\mu$  is the proper motion in arcseconds per year, has long been used as a proxy for the absolute magnitude of a star, for a sample with similar kinematics. Munn et al. (2004) presented a reduced proper motion diagram for a portion of SDSS DR1 in their Figure 12. Their SDSS+USNO-B catalog is 90% complete to  $g = 19.7$ , with proper motion errors  $\sim 3.5 \text{ mas yr}^{-1}$  in right ascension and declination. Four populations are delineated as roughly parallel diagonal distributions in their diagram. The old Population I main sequence is seen in the top right, and the Population II main sequence separates fairly cleanly to the left and extends down past  $H_g = 21$  near  $g - i = 2$ . The white dwarf sequence appears to separate to the left of the Population II subdwarfs, and an unconfirmed extension of this appears as a sequence of objects to higher  $H_g$  and redder color.

Figure 1 presents the reduced proper motion diagram for all stars in SDSS Data Release 2 (DR2; Abazajian et al. 2004) with  $15 < g < 20$  and with reliably measured proper motions greater than  $20 \text{ mas yr}^{-1}$ . Individual stars are plotted only if they are bluer than  $g - i = 0$  or if  $H_g > 15.136 + 2.727(g - i)$ , a cut which should include all white dwarfs; the remaining vast majority of stars are represented by the contours, as there are too many stars to plot individually. Spectroscopically confirmed white dwarfs, white dwarf plus M dwarf binaries, subdwarfs, and QSOs are plotted as blue triangles, green triangles, red squares, and cyan circles, respectively. The spectroscopic identifications are drawn from the SDSS Data Release 1 white dwarf catalog (Kleinmann et al. 2004) and QSO catalog (Schneider et al. 2003), and the McCook & Sion (2003) catalog. We also classified all currently available SDSS spectra for stars in the diagram with  $g - i > 0$  or  $H_g > 19$ , and which had not previously been classified (190 objects total). The expected sequences of white dwarfs (pure H atmosphere,  $\log g = 8$ ) for specific tangential velocities ( $V_T$ ) are shown as solid lines, where colors and absolute magnitudes are predicted using model atmospheres from P. Bergeron (private communication). The  $V_T = 20\text{--}40 \text{ km s}^{-1}$  curves mark the expected location of disk white dwarfs, whereas the  $V_T = 150 \text{ km s}^{-1}$  curve represents the halo white dwarfs. The

white dwarf cooling curves pass through the locus of hotter white dwarfs, then make a sharp turn due to the onset of collision-induced absorption (CIA) due to molecular hydrogen for the coolest stars with pure H atmospheres (Hansen 1998; Saumon & Jacobson 1999); this opacity depresses the  $i$  band, making the colors turn bluer.

Defining a “reliable” proper motion is important, as even a small fraction of stars with falsely measured large proper motions will scatter stars from the very densely populated subdwarf turnoff region of the reduced proper motion diagram into the sparsely populated region expected to contain the cool white dwarfs. We adopt a prescription for a reliably measured proper motion similar to that delineated by Munn et al. (2004) for their catalog: (1) the SDSS detection in both the  $g$  and  $i$  band must match the “clean” criteria as described in the DR1 documentation, (2) there must be a one-to-one match between the SDSS and USNO-B objects, and (3) the proper motion fit must have an rms residual of less than 525 mas in each coordinate. We further require the star to have been detected in all 5 epochs in USNO-B, and for the distance to the nearest neighbor with  $g < 22$  to exceed 7 arcsec. The final two requirements are based on inspection of all the plate images used in the USNO-B catalog for a subsample of 562 stars in the portion of the reduced proper motion diagram expected to be populated by halo and cool disk white dwarfs ( $-1 < g < 1.5$  and  $H_g > 18$ ), and with proper motions greater than  $100 \text{ mas yr}^{-1}$  (the reality of measured proper motions smaller than that were too difficult to judge using the quick by-eye inspections we employed). Of the 201 inspected stars that were detected in all 5 USNO-B epochs, and whose nearest neighbor (brighter than  $g = 22$ ) is greater than 7 arcsec away, only 3 were judged to have a falsely measured large proper motion, for a 1.5% contamination rate. On the other hand, of the 20 inspected stars that were detected in all 5 USNO-B epochs but had a neighbor closer than 7 arcsec, 7 were judged to have an incorrectly measured proper motion, for a contamination rate of 35%. Objects separated by less than 7 arcsec tend to be blended on the Schmidt plates, leading to incorrectly measured proper motions. All of the 208 inspected stars which were not detected in one or two of the USNO-B epochs and which have a nearest neighbor closer than 7 arcsec had incorrectly measured proper motions. Even if the nearest neighbor is greater than 7 arcsec away, the contamination rate of falsely measured large proper motions increases for stars not detected in all 5 USNO-B epochs. For such stars, 20 of 39 inspected stars not detected in one of the USNO-B epochs had incorrectly measured proper motions, for a contamination rate of 51%, while 81 of 91 not detected in two of the USNO-B epochs had incorrectly measured proper motions, for a contamination rate of 89%.

In Figure 1, it is clear that the hot white dwarfs previously targetted spectroscopically by SDSS are well separated from main sequence and subdwarf stars (represented by the contours) and are located where expected from the models. It is also clear that the white dwarf locus extends redder and to larger reduced proper motion, well separated from the

subdwarf locus (the diagonal cut where we start to plot individual stars), and that SDSS has not spectroscopically observed these cooler white dwarf candidates. This drove our target selection. Our goal was to obtain spectroscopic identifications for a large sample of cool white dwarf candidates so as to understand the efficiency of using reduced proper motions to select cool white dwarfs as well as the contamination due to subdwarfs. Thus we selected most of our targets from the region with  $g-i > 0$  and to the left of the  $V_T = 20 \text{ km s}^{-1}$  curve, though we also selected some to the right of the curve to better understand how cleanly the white dwarf and subdwarf loci separate.

### 3. Observations

Follow-up spectroscopy of the cool white dwarf candidates were obtained at the HET, the MMT, and the McDonald 2.7m Harlan Smith Telescope between September 2003 and October 2004 (an additional observing run with the Kitt Peak 4m Telescope was completely lost to weather). We used the HET equipped with the Marcario Low Resolution Spectrograph (LRS) to obtain low resolution spectroscopy of 22 cool white dwarf candidates. Grism 2 with a 1.5" slit produced spectra with a resolution of 6 Å over the range 4280 – 7340 Å. Spectroscopy for 56 additional stars was obtained at the MMT with the Blue Channel Spectrograph and the 500 l/mm grating, which produced spectra with a resolution of 3.6 Å over the range 3640 – 6800 Å. In addition, we obtained spectroscopy for 89 stars at the McDonald 2.7m Telescope with the Large Cassegrain Spectrograph (LCS) and TI1 camera using grating No. 43 (600 l/mm), which produced spectra with a resolution of 5.2 Å over the range 3870 – 5260 Å. In each case, a spectrophotometric standard star was observed each night for flux calibration. Ne–Cd, He–Ar–Ne, and Ar calibration lamp exposures were taken after each observation with the HET, the MMT, and the McDonald 2.7m, respectively. The data were reduced using standard IRAF<sup>1</sup> routines.

The spectra for all of the observed white dwarfs at the HET, the MMT, and the McDonald 2.7m are shown in Figures 2, 3, and 4, respectively. The spectra are ordered in decreasing  $g - r$  color for Figures 2 and 3, and decreasing  $u - r$  color for Figure 4. The majority of the objects observed at the HET and the MMT are featureless cool DC white dwarfs. The only features seen in these spectra are due to sky subtraction problems at 5577, 5890/5896, 6300, and the atmospheric  $B$  band at 6890 Å. Several white dwarfs show only a

---

<sup>1</sup>IRAF is distributed by the National Optical Astronomy Observatory, which is operated by the Association of Universities for Research in Astronomy (AURA), Inc., under cooperative agreement with the National Science Foundation.

weak H $\alpha$  line and are DA white dwarfs with probable cool, H-rich atmospheres. Most of the brighter objects observed at the McDonald 2.7m are DA white dwarfs. Three objects clearly show additional features due to late type star companions (J0929+5547, J1336+0017, J2340-1106). Two objects observed at the 2.7m are magnetic DAs (J1011+0029, J1144+6629), while two other objects observed at the 2.7m and an additional three objects observed at the MMT are DZAs with detectable Ca II H and K lines and Balmer lines (J0045+1420, J0748+3506, J1627+4859, J1654+3829, J2154+1300). We also note that four previously known white dwarfs, namely SDSS J0109-1042 (LP707-8), J0755+3621 (WD0752+365), J1025+0043 (LHS 282), and J1145+6305 (WD1143+633) were observed at the MMT and the McDonald 2.7m, and are included in Figures 3 and 4.

The biggest difficulty in classifying the spectra is to distinguish DZ, DZA and DAZ white dwarfs<sup>2</sup> with refractory heavy elements from nondegenerate probable-main sequence stars (subdwarf F, G, and K types) with low, scaled-solar heavy elements. Ca appears most frequently in DZ, DAZ and DZA stars, followed by Mg, Fe and occasionally Na. The white dwarfs apparently never show the CH band (4300 Å) which is detected for sdG and cooler stars ( $g - i > 0.4$ ), and do not show MgH and CaH which appear in progressively-cooler sdK stars.

Figure 5 shows the spectra for several subdwarfs observed at the MMT. The spectra are plotted in order of decreasing  $T_{\text{eff}}$ , represented by increasing  $g - i$  color. This figure demonstrates that subdwarfs have Ca II (hence need MMT and McDonald 2.7m blue coverage), and usually many other metal features plus the CH molecular band. Additional MgH and CaH bands can be seen among cooler subdwarfs (without enough blue coverage, HET was mostly used to observe cool white dwarf candidates with similar colors to G and K type subdwarfs). We paid close attention to the  $u - g$  and  $g - r$  colors of each star, comparing colors of each candidate with white dwarf model colors to see if they were consistent with the strengths of the H lines, and the degree to which cool DA Balmer decrements steepen until for the coolest DA's only H $\alpha$  is seen.

Our classifications and additional data for the 112 spectroscopically-confirmed white dwarfs and 55 subdwarfs from this study are given in Tables 1 and 2, respectively. Positions are those from the SDSS Astrometric pipeline (Pier et al. 2003). The photometric calibration is based on the SDSS standard star system (Smith et al. 2002) tied to the survey data with the Photometric Telescope (Hogg et al. 2001). Interstellar absorption  $A_u$  from Schlegel, Finkbeiner & Davis (1998), and fully dereddened magnitudes and colors are given for each

---

<sup>2</sup>Note that the difference between DAZ and DZA stars is whether the dominant atmospheric constituent is hydrogen or helium, respectively. DZA stars show steep Balmer decrements at higher  $T_{\text{eff}}$  than DAZ stars.

object. Tables 1 and 2 also give the proper motions in each component and the number of epochs in which an object is detected. In addition, the effective temperatures, photometric distances and the tangential velocities for the newly discovered cool white dwarfs (see §4.4) are also given in Table 1.

A few stars in Table 1 were previously known as likely white dwarfs. The most certain case is SDSS J131313.12+022645.8 (LHS2696) which has a (preliminary) parallax in Dahn et al. (1989). There are 13 additional stars discovered in the NLTT catalog, (Luyten 1979), most with Luyten color class a, f, or g, that would have been considered to be nearly certain white dwarfs on the basis of the NLTT data alone; the spectra in this paper now confirm these classifications. The one very cool white dwarf in Table 1 that is also in the NLTT catalog is SDSS J075313.28+423001.6 (LP207-50). It has color class m in the NLTT, so would not be considered as a white dwarf from the NLTT data alone. In addition, three stars in Table 1 were identified from their proper motion by Lépine et al. (2003): SDSS J100225.85+610858.1 (LSR 1002+6108), SDSS J110731.38+485523.0 (LSR 1107+4855), and SDSS J222233.90+122143.0 (LSR 2222+1221). The first two were classified as probably white dwarfs and the third as probably a subdwarf on the basis of their reduced proper motion and photographic colors.

## 4. Results

### 4.1. Reduced Proper Motion Diagram

Figure 6 repeats the reduced proper motion diagram of Figure 1, except that the spectroscopic identifications presented in this paper are indicated rather than previously known identifications. Again, this is limited to stars with reliable proper motions; that is, stars detected in all 5 USNO-B epochs and with no neighbor brighter than  $g = 22$  within 7 arcsec. There is a clean separation between the white dwarfs and subdwarfs. Of the 95 spectroscopically confirmed stars bluer than  $g - i = 1.5$  and below the  $V_T = 20 \text{ km s}^{-1}$  curve, corresponding to the region we expect to find only white dwarfs, 91 are certain white dwarfs, 2 are certain subdwarfs, and two are probable white dwarfs for which a classification of subdwarf can not be ruled out. Visual inspection of the plate images reveals that the two subdwarfs had falsely measured large proper motions, consistent with the contamination rate derived earlier for our adopted reliable proper motion criteria, while the two probable white dwarfs had correctly measured proper motions.

Figure 7 shows the MMT spectra for these 2 probable white dwarfs. SDSS J2236+1419 ( $H_g = 18.75$  and  $g - i = 0.52$ ) shows Mg I 3830, Ca II 3933, 3968, Ca I 4226, Na I 5892

and probable Mg I 5175 with no detectable H $\alpha$ , H $\beta$ , and CH band. The absent H and CH features suggest a very non-Population II (scaled solar) metallicity DZ white dwarf. SDSS J1214+6216 ( $H_g = 21.97$  and  $g - i = 0.64$ ) shows Mg I 3830, Ca II, no Ca I, no CH, weak H-beta, possible Na I 5892, and rather strong H-alpha. The steep H decrement is consistent with a cool white dwarf with pressure-broadening, quenching the higher Balmer levels. Again, the absent CH is probably inconsistent with an sdG. We classify this object as a probable DZA white dwarf, pending detailed analysis. Assuming that these two objects are white dwarfs, we find no contamination from subdwarfs with correctly measured proper motions. On the other hand, if we assume that these objects are in fact subdwarfs, they would represent subdwarfs that truly have scattered into the cool white dwarf region of the reduced proper motion diagram; there is still potential for some genuine contamination from subdwarfs.

We also observed stars that did not meet our criteria for a reliable proper motion, having either not been detected in 1 or 2 USNO-B epochs or having a neighbor within 7 arcsec. Of these, 16 were white dwarfs (plotted as blue asterisks in Figure 6), all located within the white dwarf region of the reduced proper motion diagram; upon visual inspection of the plates used in USNO-B, all of the measured proper motions were correct. Another 37 were subdwarfs (see Table 2), located both in the white dwarf and subdwarf regions of the reduced proper motion diagram; visual inspection shows all but three of these to have incorrectly measured proper motions, and the proper motions of the remaining three were too small to determine their validity by eye.

The reduced proper motion diagram, using our conservative criteria for a reliable proper motion, can thus be used to define a statistically complete sample of white dwarfs, including the coolest white dwarfs which are difficult to efficiently select using other techniques. There is a roughly 1.5% contamination rate of incorrectly measured proper motions. There is likely no contamination due to subdwarfs with correctly measured proper motions, though contamination of a few percent is still possible. True white dwarfs that fail to meet the proper motion criteria must be accounted for, either statistically or by using visual inspection to verify proper motions for all candidates. This result is used in Harris et al. (2005) to construct the white dwarf luminosity function using the SDSS Data Release 3 imaging and USNO-B astrometry.

## 4.2. Color-Color Diagrams

SDSS color-color diagrams for spectroscopically identified proper motion objects are shown in Figure 8. The spectral classifications are indicated in the diagrams, and contours



that show the colors of nondegenerate stars in the SDSS are included for comparison. The curves show the colors of white dwarf model atmospheres of pure H (solid curves) and pure He (dashed curves) composition with  $\log g = 7, 8, \text{ and } 9$ , kindly made available to us by P. Bergeron.

Harris et al. (2003) showed that the sequence of white dwarfs hotter than 12,000 K is contaminated only by hot subdwarfs. Our  $u - g$  vs.  $g - r$  color-color diagram demonstrates that white dwarfs and subdwarfs selected from the reduced proper motion diagram separate from each other for  $u - g \leq 1.0$ , though this result depends on a handful of white dwarfs observed between the range  $0.6 \leq u - g \leq 1.0$  and further observations are needed to confirm this result.

Figure 8a also shows that the cool white dwarf model atmospheres cannot predict the  $u - g$  colors below 6,000 K accurately, though the  $g - r$ ,  $r - i$ , and  $i - z$  colors agree reasonably well with the observed sequence of cool white dwarfs (see Figures 8b and 8c). Bergeron, Leggett, & Ruiz (1997) were the first to introduce a UV opacity source in the coolest hydrogen-rich white dwarf models in terms of a pseudo continuum opacity to fit the observed hydrogen-rich cool white dwarf sequence. They found that this opacity source is needed to explain the observed UV colors of cool hydrogen-rich white dwarfs below 5,300 K. This is also seen in the  $B - V$  vs.  $V - K$  color-color diagram of Bergeron, Ruiz, & Leggett (2001), and  $r - DDO51$  vs.  $r - z$  color-color diagram of Kilic et al. (2004). Wolff, Koester, & Liebert (2002) showed that this UV flux deficiency (relative to model atmosphere predictions) extends even more strongly into the space ultraviolet region (2000 – 3200 Å). Here, we find that the  $u - g$  colors for neither cool DA nor cool DC white dwarfs can be explained with the current model atmospheres. Significant improvements are needed in the cool white dwarf model atmospheres to understand the unexplained UV opacity which is crucial for the coolest white dwarfs. In fact, this may be the reason why efforts to fit the spectral energy distributions of ultracool white dwarfs fail.

The majority of the cool white dwarfs with  $r - i > 0.25$  ( $T_{\text{eff}} < 5000\text{K}$ ) tend to have bluer  $i - z$  colors compared to the model predictions (see Figure 8c); the observed blue turn-off of cool white dwarfs is at a bluer color than expected from the models. All but four of the cool white dwarfs occupy a region to the left of the  $\log g = 9$  (left-most line) white dwarf models. This implies that either all of the very cool white dwarfs are massive, they have mixed H/He atmospheres, or our understanding of the CIA opacities are incomplete. All being massive is statistically unlikely as the average mass for the cool white dwarfs ( $T_{\text{eff}} \leq 5000\text{K}$ ) with trigonometric parallax measurements is  $0.61 \pm 0.2 M_{\odot}$  (Bergeron, Leggett, & Ruiz 2001). Mixed atmosphere white dwarfs are expected to show stronger flux deficits in the infrared than pure H white dwarfs (Bergeron, Saumon, & Wesemael 1995); the effects of CIA becomes

significant at warmer temperatures, which could explain the observed blue turn-off of cool white dwarfs in Figure 8c. Bergeron & Leggett (2002) argued that all white dwarfs cooler than 4000 K have mixed H/He atmospheres. In addition, Kilic et al. (2004) suggested that all white dwarfs cooler than 5000 K may have mixed atmospheres. Therefore, this figure presents further evidence that the coolest white dwarfs indeed have helium rich atmospheres.

### 4.3. Non-DA Gap

The  $H\alpha$  and  $H\beta$  equivalent widths of all DA and DC white dwarfs in our sample are shown against  $g - r$  in Figure 9. White dwarf models predict  $H\alpha$  to disappear around  $V - I \sim 1.1$  (see Figure 7 of Bergeron, Ruiz, & Leggett 1997). Although there is a large scatter in our equivalent width measurements in Figure 9, it is apparent that the  $H\alpha$  and  $H\beta$  equivalent widths decrease with increasing  $g - r$  color and they vanish around  $g - r \sim 0.7$  (or  $V - I \sim 1.1$ ), in good agreement with the model predictions. The scatter in the equivalent width measurements may partly be due to variations in gravities and the use of spectra with different signal-to-noise ratios from four different telescope + instrument combinations.

Bergeron, Ruiz & Leggett (1997) and Bergeron, Leggett & Ruiz (2001) argued that most of the white dwarfs with  $T_{\text{eff}}$  in the range 6000 K – 5000 K are of DA type, and they found evidence for a so-called non-DA gap. Even though non-DA stars are seen above and below this temperature range, they found only two peculiar non-DA stars inside the gap. Bergeron, Ruiz & Leggett (1997), Bergeron, Leggett & Ruiz (2001), and Hansen (1999) tried to explain the existence of this gap in terms of different physical mechanisms, i.e. convective mixing and different evolutionary timescales of hydrogen-rich and helium-rich white dwarfs. The existence of the non-DA gap is apparent in Bergeron, Leggett & Ruiz’s (2001)  $V - I$  vs.  $V - K$  color-color diagram. Figure 10 shows  $u - g$  vs.  $g - r$  (left panel),  $g - r$  vs.  $r - i$  (middle panel), and  $r - i$  vs.  $i - z$  (right panel) color-color diagrams for white dwarfs in our sample. The data set is divided into DA (upper panels) and non-DA (lower panels, DC and DQ) stars. The pure H (DA panels) and pure He (non-DA panels) model sequences with  $6000K \gtrsim T_{\text{eff}} \gtrsim 5000K$  are also shown for  $\log g = 7$  (solid line),  $\log g = 8$  (dashed line), and  $\log g = 9$  (dotted line). The two differences between these color-color diagrams and Figure 8 are that (1) DC white dwarfs discovered at the McDonald 2.7m are not included in Figure 10 since the 2.7m spectra do not cover  $H\alpha$ , and so some of the white dwarfs observed with the 2.7m and classified as DCs may turn out to be DAs showing  $H\alpha$  only, and (2) ultra-cool white dwarfs discovered in the SDSS are not included. SDSS J1001+3903, an ultra-cool white dwarf discovered by Gates et al. (2004), falls in the non-DA gap in the  $u - g$  vs.  $g - r$  diagram, but not in the other two diagrams. Even though ultra-cool white dwarfs are

predicted to have  $T_{\text{eff}} \leq 4000K$ , they mimic bluer/warmer objects in the various color-color diagrams and therefore are not included in this discussion.

DA white dwarfs show  $H\alpha$  absorption for  $g - r \leq 0.7$  ( $\geq 5000K$ ) and we should have detected  $H\alpha$  for DCs with  $6000K \gtrsim T_{\text{eff}} \gtrsim 5000K$  if they had pure H atmospheres. The  $H\alpha$  panel in Figure 9 shows exactly 3 DC stars in the gap (The gap, marked by the dashed lines, is  $g - r = 0.39$  to  $0.64$  for hydrogen atmospheres). Based on *ugriz* photometry (Figure 10), we see DC stars above and below the non-DA gap, but we find only 3 to 5 DC stars (shown as filled red circles in lower panels) in the gap. All of these white dwarfs (SDSS J0157+1335, J1203+0426, J1205+0449, J1648+3939, J1722+5752) are observed at the MMT and HET, and Balmer lines cannot be seen in their spectra. Assuming pure He composition, we estimate their temperatures to be  $5254K$ ,  $5144K$ ,  $5635K$ ,  $5536K$ , and  $5555K$  (see the next section for temperature estimates). These stars appear to be non-DA stars in the 5000-6000K temperature range, and fill in the Bergeron et al non-DA gap to some extent. The fraction of DA/non-DA stars in this temperature range is still seen to be large in our data, and further data are needed to quantify the ratio. Moreover, Bergeron, Ruiz & Leggett (1997) have identified a group of DC white dwarfs which lie close to  $T_{\text{eff}} = 6000K$  whose energy distributions are better reproduced with pure hydrogen models. Therefore, some or all of these stars may be explained with H-rich compositions. Bergeron, Leggett, & Ruiz (2001) and Ruiz & Bergeron (2001) showed that infrared photometry is needed to discriminate between between hydrogen-rich and helium-rich atmospheres for cool white dwarfs; infrared photometry is needed to reliably determine the spectral types and temperatures for these stars. In any case, our data supports at least a deficit in the number of non-DA white dwarfs in the predicted non-DA gap.

#### 4.4. Model Atmosphere Analysis

The  $u, g, r, i,$  and  $z$  photometry for each of the new spectroscopically confirmed white dwarfs has been fitted with synthetic photometry predicted from the model atmospheres (P. Bergeron, private communication), using a minimum chi square fit. Since trigonometric parallax measurements are not available for these white dwarfs, a value of  $\log g = 8.0$  has been assumed for all objects. Due to larger uncertainties in  $u$  and  $z$ , and the fact that the  $u$  magnitudes of cool white dwarfs are affected by an unexplained UV opacity source,  $u$  and  $z$  magnitudes are given lower weight in our fits. The fits have been done using only  $u, g,$  and  $r$  magnitudes for white dwarf + late type star binaries, though some of these binaries may have contaminated  $u, g,$  and  $r$  magnitudes.

While spectra of bluer white dwarfs allow us to determine whether the atmosphere is

hydrogen-rich or helium-rich,  $H\alpha$  and  $H\beta$  disappear around  $g - r \sim 0.7$  and so IR photometry is needed to determine the atmospheric composition for DCs. We assume hydrogen-rich composition for the analysis of all of the DA and DC white dwarfs in our sample. Figure 11 shows the effects of using hydrogen-rich versus helium-rich composition models on our temperature estimates for the DC stars in our sample. Both hydrogen-rich and helium-rich models give similar answers for stars with  $T_{\text{eff}}$  in the range 10000 – 5500 K ( $g - i < 0.7$ ), though the effect drastically increases below 5500K due to the onset of collision induced absorption. Pure He models predict warmer temperatures than the pure H models; the optical colors of a 4000 K pure H atmosphere white dwarf can be fit with a 4700 K pure He white dwarf model.

We assumed zero reddening for white dwarfs with estimated distances  $\leq 100$  pc, and used the full reddening value from Schlegel, Finkbeiner, & Davis (1998) if the estimated distance from the Galactic plane is larger than 250 pc. For white dwarfs with estimated distances between 100 and 250 pc, we used a linear interpolation between zero and the full reddening coefficient.

Results of the model atmosphere fits are summarized in columns 12–16 of Table 1. For each white dwarf, we give (assuming pure H composition with  $\log g = 8.0$ ) the effective temperature, the predicted bolometric magnitude, the absolute magnitude in  $g$ , the distance, and the estimated tangential velocity. According to our fits, there are seven white dwarfs with  $T_{\text{eff}} \leq 4,000$  K in our sample, but these temperature estimates are questionable, and IR photometry is needed to obtain reliable results for these objects. Although most of the newly found white dwarfs show disk kinematics, there are 16 objects with  $V_T \geq 150$  km s $^{-1}$  that may be halo white dwarfs. Halo membership of these objects and several others from the SDSS Data Release 3 are discussed in Harris et al. (2005).

## 5. Conclusions and Future Work

SDSS photometry and SDSS+USNO-B astrometry (Munn et al. 2004) has been used to isolate cool white dwarf candidates in a reduced proper motion diagram in the SDSS Data Release 2. Using SDSS spectra and follow-up spectroscopy on the MMT, HET, and the McDonald 2.7m, we showed that the white dwarf locus in the reduced proper motion diagram is cleanly separated from the far more numerous subdwarfs, with a contamination rate due to falsely measured large proper motions of only 1–2%. In a companion paper, Harris et al. (2005) use this clean separation of white dwarfs in the reduced proper motion diagram to assemble a statistically complete sample of white dwarfs in the SDSS Data Release 3 and determine the white dwarf luminosity function. The detailed shape of this

new luminosity function will eventually make it possible to study the cooling physics of white dwarfs in detail, e.g. neutrino cooling, crystallization, and phase separation. These effects produce overlapping signatures (bumps) in the white dwarf luminosity function which can be used to calibrate their significance. The details of these constituent input physics can affect the implied ages of cool white dwarfs below  $\log(L/L_{\odot}) \sim -4.2$  by as much as 2-3 Gyr (Hawkins & Hambly 1999; Montgomery et al. 1999; Salaris et al. 2000).

All of the ultracool white dwarfs discovered in SDSS (Harris et al. 2001; Gates et al. 2004) show significant proper motion, hence they would be discovered in our proper motion survey if not targeted by SDSS fiber spectroscopy. We have discovered seven new cool white dwarfs with estimated temperatures below 4000 K. Nevertheless, these objects may have temperatures above 4000 K if they have pure He atmospheres (see Figure 11). Our spectroscopy at the HET and the MMT do not go red enough to detect the CIA in the near IR, though all of these objects and several others should show infrared flux deficiency due to CIA if they have pure H or mixed H/He atmospheres. Our SDSS DR2 proper motion catalog does not reveal any other ultracool white dwarf candidate exhibiting strong CIA absorption. Therefore, SDSS1337+00, LHS3250 and SDSSJ0947+44 are the only ultracool white dwarfs (within our magnitude limit) showing strong CIA absorption in the SDSS DR2 imaging area (3324 square degrees). Further progress in understanding the ultracool white dwarfs and estimating reliable temperatures for our cool white dwarf sample can be achieved with the help of *JHK* infrared photometric observations. We have begun such a program at the NASA Infrared Telescope Facility. Trigonometric parallax measurements for these white dwarfs will also be necessary to measure their masses.

Even though our survey has a fainter magnitude limit and a lower proper motion cut off than the LHS survey, the faint end of the white dwarf luminosity function where most of the age sensitivity resides is still poorly populated. The magnitude limit of the SDSS+USNO-B proper motion catalog is set by the photographic POSS I and POSS II plates. Although SDSS imaging is 95% complete down to  $g = 22$ , the SDSS+USNO-B proper motion catalog is only 90% complete down to  $g = 19.7$ . A second epoch CCD imaging survey in  $r$  or  $i$  to 22 mag may be necessary to find the coolest white dwarfs in the disk and possible halo white dwarfs (von Hippel et al. 2004). Also, we may be missing slowly moving cool white dwarfs; a kinematically unbiased control sample, e.g. DDO51 photometry + multi object spectroscopy (Kilic et al. 2004), would be useful to check the completeness of our survey.

This material is based upon work supported by the National Science Foundation under Grants AST-0307315 (to TvH, DEW, and MK) and AST-0307321 (to JL and KAW). We thank Pierre Bergeron and Didier Saumon for making their model atmospheres available to us. We also thank Harry Shipman for careful reading of this manuscript. The Hobby-Eberly

Telescope (HET) is a joint project of the University of Texas at Austin, the Pennsylvania State University, Stanford University, Ludwig-Maximilians-Universität München, and Georg-August-Universität Göttingen. The HET is named in honor of its principal benefactors, William P. Hobby and Robert E. Eberly. The Marcario Low Resolution Spectrograph is named for Mike Marcario of High Lonesome Optics who fabricated several optics for the instrument but died before its completion. The LRS is a joint project of the Hobby-Eberly Telescope partnership and the Instituto de Astronomia de la Universidad Nacional Autonoma de México.

Funding for the Sloan Digital Sky Survey (SDSS) has been provided by the Alfred P. Sloan Foundation, the Participating Institutions, the National Aeronautics and Space Administration, the National Science Foundation, the U.S. Department of Energy, the Japanese Monbukagakusho, and the Max Planck Society. The SDSS Web site is <http://www.sdss.org/>.

The SDSS is managed by the Astrophysical Research Consortium (ARC) for the Participating Institutions. The Participating Institutions are The University of Chicago, Fermilab, the Institute for Advanced Study, the Japan Participation Group, The Johns Hopkins University, the Korean Scientist Group, Los Alamos National Laboratory, the Max-Planck-Institute for Astronomy (MPIA), the Max-Planck-Institute for Astrophysics (MPA), New Mexico State University, University of Pittsburgh, Princeton University, the United States Naval Observatory, and the University of Washington.

## REFERENCES

- Abazajian, K. et al. 2004, *AJ*, 128, 502
- Abazajian, K. et al. 2003, *AJ*, 126, 2081
- Bergeron, P., Saumon, D., & Wesemael, F. 1995, *ApJ*, 443, 764
- Bergeron, P., Ruiz, M. T. & Leggett, S. K. 1997, *ApJS*, 108, 339
- Bergeron, P., Leggett, S. K. & Ruiz, M. T. 2001, *ApJS*, 133, 413
- Bergeron, P. 2003, *ApJ*, 586, 201
- Claver, C. F. 1995, Ph.D. Thesis, University of Texas
- Dahn, C.C., Monet, D.G., & Harris, H.C. 1989, in *IAU Colloq. 114, White Dwarfs*, ed. G. Wegner (Berlin, Springer), 24
- Davies, M. B., King, A., & Ritter, H. 2002, *MNRAS*, 333, 463

- Fan, X. 1999, *AJ*, 117, 2528
- Gates, E. et al. 2004, *ApJ*, 612, 129
- Hansen, B. M. S. 1998, *Nature*, 394, 860
- Hansen, B. M. S. 2003, *ApJ*, 582, 915
- Harris, H. C. et al. 2001, *ApJ*, 549, 109
- Harris, H. C. et al. 2003, *AJ*, 126, 1023
- Harris, H. C. et al. 2005, *AJ*, submitted
- Hogg, D. W. 2001, *AJ*, 122, 2129
- Kilic, M., Winget, D.E., von Hippel, T., & Claver, C.F. 2004, *AJ*, 128, 1825
- Kleinman, S. J. et al. 2004, *ApJ*, 607, 426
- Lépine, S., Shara, M.M., & Rich, R.M. 2003, *AJ*, 126, 921
- Liebert, J. 1979, In *IAU Colloquium 53: White Dwarfs and Variable Degenerate Stars*, p. 146
- Liebert, J., Dahn, C. C., & Monet, D. G. 1988, *ApJ*, 332, 891
- Liebert, J., Bergeron, P., & Holberg, J. 2005, *ApJS*, in press
- Luyten, W. J. 1979, *LHS Catalogue. A Catalogue of Stars with Proper Motions Exceeding 0.5" Annually* (Minneapolis: Univ. Minnesota)
- Luyten, W.J. 1979, *NLTT Catalogue* (Minneapolis: Univ. Minnesota Press) (NLTT)
- Luyten, W.J. 1918, *Lick Observatory Bulletin*, 10, 135
- McCook, G. P. & Sion, E. M. 2003, *VizieR On-line Data Catalog: III/235*
- Monet, D. G., et al. 2003, *AJ*, 125, 984
- Monet, D. B. A. et al. 1998, *VizieR Online Data Catalog*, October, 1252
- Montgomery, M. H., Klumpe, E. W, Winget, D. E., & Wood, M. A. 1999, *ApJ*, 525, 482
- Munn, J. A. et al. 2004, *AJ*, 127, 3034

- Oppenheimer, B. R. Hambly, N. C. Digby, A. P. Hodgkin, S. T. & Saumon, D. 2001, *Science*, 292, 698
- Oswalt, T. D., Smith, J. A., Wood, M. A., & Hintzen, P. 1996, *Nature*, 382, 692
- Pier, J. R. et al. 2003, *AJ*, 125, 1559
- Reid, I. N., Sahu, K.C., & Hawley, S.L. 2001, *ApJ*, 559, 942
- Reyle, C., Robin, A. C., & Creze, M. 2001, *A&A*, 378, 53
- Ruiz, M. T. & Bergeron, P. 2001, *ApJ*, 558, 761
- Salaris, M., García-Berro, E., Hernanz, M., Isern, J., & Saumon, D. 2000, *ApJ*, 544, 1036
- Saumon, D. & Jacobson, S. B. 1999, *ApJ*, 511, 107
- Schlegel, D. J., Finkbeiner, D. P., & Davis, M. 1998, *ApJ*, 500, 525
- Schmidt, G. D. 2003, *ApJ*, 595, 1101
- Schneider, D. P. et al. 2003, *AJ*, 126, 2579
- Silvestri, N. M., Oswalt, T. D., & Hawley, S. L. 2002, *AJ*, 124, 1118
- Smith, J. A. et al. 2002, *AJ*, 123, 2121
- Spagna, A., Carollo, D., Lattanzi, M. G., & Bucciarelli, B. 2004, *A&A*, 428, 451
- Stoughton, C. et al. 2002, *AJ*, 123, 485
- von Hippel, T. et al. 2004, in *The XIV European Workshop on White Dwarfs*, ed. D. Koester & S. Moehler, in press
- Winget, D. E., Hansen, C. J., Liebert, J., Van Horn, H. M., Fontaine, G., Nather, R. E., Kepler, S. O., & Lamb, D. Q. 1987, *ApJ*, 315, L77
- Wolff, B., Koester, D., & Liebert, J. 2002, *A&A*, 385, 995
- York, D. G. et al. 2000, *AJ*, 120, 1579



Table 1. Spectroscopically Identified White Dwarfs

Name (SDSS J)	$g$	$u - g$	$g - r$	$r - i$	$i - z$	$A_{\text{H}}$	$\mu_{\text{ra}}$	$\mu_{\text{dec}}$	Ep	Type	$T_{\text{eff}}$	$M_{\text{bol}}$	$M_{\text{g}}$	D	$V_{\text{T}}$	Source
00 03 16.69-01 11 17.9	19.21	1.22	0.49	0.22	0.02	0.16	98	-16	6	DA	5351	14.57	15.14	69.19	32.57	MMT
00 11 42.67-09 03 24.3	17.73	0.64	0.31	0.12	0.01	0.21	4	-134	6	DA	6125	13.97	14.37	50.31	31.97	2.7m
00 28 37.06-00 29 28.9	19.68	0.54	0.36	0.04	-0.11	0.10	103	67	6	DC	6381	13.80	14.16	128.79	75.01	HET
00 43 16.02+15 40 59.5	18.11	0.53	0.18	0.01	-0.05	0.28	-37	25	6	DA	6844	13.49	13.82	79.16	16.76	2.7m
00 45 21.88+14 20 45.3	18.81	1.35	0.63	0.21	0.03	0.55	260	-53	6	DZA	4732	15.11	15.90	45.73	57.51	MMT
01 02 59.98+14 01 08.1	19.29	1.71	0.73	0.27	0.11	0.22	12	106	6	DC	4582	15.25	16.10	46.84	23.68	MMT
01 15 14.73+14 35 57.5	18.54	0.52	0.25	0.09	-0.02	0.31	-45	-55	4	DA	6320	13.84	14.21	81.60	27.49	MMT
01 28 27.47-00 45 12.6	17.74	1.02	0.37	0.15	0.00	0.16	147	-43	6	DA	5854	14.18	14.62	44.54	32.33	2.7m
01 57 43.25+13 35 58.2	19.15	1.19	0.64	0.16	0.05	0.25	87	-62	6	DC	5040	14.84	15.51	57.63	29.18	MMT
01 59 38.43-08 12 42.4	19.80	0.42	0.09	-0.10	0.01	0.13	322	-119	6	DA	8214	12.69	13.01	230.40	374.90	MMT
02 50 05.81-09 10 02.8	18.87	1.06	0.48	0.18	0.05	0.15	106	DA	6	DA	5474	14.47	15.00	62.59	31.45	MMT
02 56 41.62-07 00 33.8	18.81	1.73	0.80	0.34	0.08	0.26	373	-202	6	DC	4211	15.62	16.56	30.94	62.22	MMT
02 58 54.42+00 30 40.4	18.84	0.73	0.27	0.06	-0.07	0.42	-80	16	6	DA	6189	13.93	14.32	92.32	35.70	MMT
03 09 24.87+00 25 25.3	17.75	0.84	0.34	0.13	-0.02	0.57	-6	-106	6	DC	5637	14.34	14.83	46.60	23.45	2.7m
03 14 49.81-01 05 19.3	18.31	0.88	0.38	0.12	-0.04	0.39	-77	-71	6	DA	5709	14.29	14.76	58.48	29.03	2.7m
03 16 13.90-08 16 37.6	16.63	0.56	0.17	0.02	-0.04	0.48	90	-103	6	DA	6610	13.64	13.99	39.65	25.71	2.7m
03 30 54.88+00 37 16.5	19.33	0.81	0.34	0.10	0.01	0.57	77	34	6	DA	5690	14.30	14.78	98.78	39.41	MMT
04 06 32.39-04 32 50.4	17.02	0.53	0.17	0.00	-0.10	0.56	171	80	6	DA	6624	13.63	13.98	48.89	43.75	2.7m
04 06 47.32-06 44 36.9	17.70	0.74	0.34	0.07	0.03	0.45	67	27	6	DA	5884	14.15	14.59	48.70	16.67	2.7m
07 48 11.90+35 06 32.4	18.08	1.13	0.36	0.09	-0.07	0.30	-44	-141	6	DZA	5925	14.12	14.55	56.16	39.32	2.7m
07 53 13.28+42 30 01.6	17.91	1.84	0.84	0.30	0.10	0.23	113	-403	6	DC	4226	15.61	16.54	20.36	40.39	2.7m
07 56 31.11+41 39 50.9	16.76	0.52	0.18	0.03	-0.05	0.20	-9	-349	6	DA	6951	13.42	13.75	42.59	70.48	2.7m
08 20 36.99+43 10 05.3	17.40	0.49	0.08	0.03	-0.09	0.33	-63	-103	6	DA	7192	13.27	13.59	64.72	37.04	2.7m
08 20 56.07+48 03 52.9	17.16	0.62	0.24	0.12	-0.06	0.22	224	-80	6	DA	6388	13.79	14.16	42.91	48.37	2.7m
08 23 07.81+48 33 16.6	17.79	0.74	0.25	0.10	-0.02	0.22	-217	-72	6	DA	6378	13.80	14.16	57.26	62.06	2.7m
08 25 19.70+50 49 20.1	19.17	1.72	0.86	0.33	0.05	0.24	-331	-330	6	DC	4048	15.79	16.74	33.42	74.04	MMT
08 36 41.56+45 56 58.7	19.89	1.63	0.84	0.27	0.15	0.15	-64	-169	6	DC	4373	15.46	16.36	53.19	45.56	MMT
08 37 12.30+46 13 25.1	18.39	0.69	0.29	0.09	0.00	0.14	-80	-40	6	DA	6363	13.81	14.18	72.90	30.90	MMT
09 19 48.92+01 13 53.0	18.21	0.73	0.30	0.11	0.00	0.13	137	-193	6	DA	6227	13.90	14.29	63.81	71.58	2.7m
09 29 03.12+55 47 58.5	17.85	0.43	0.23	1.05	0.87	0.15	-350	-18	6	DA+M	6719	13.57	13.91	64.55	107.23	2.7m
09 34 38.94+53 29 37.4	17.47	0.51	0.20	0.04	-0.01	0.06	-151	-145	6	DA	6976	13.40	13.73	57.12	56.68	2.7m
09 42 44.96+44 37 43.1	19.44	1.92	0.88	0.37	0.19	0.06	-135	-189	6	DC	4052	15.79	16.73	35.66	39.25	HET
10 01 19.48+46 56 50.6	19.24	2.06	1.06	0.33	0.09	0.07	-17	-339	6	DC	3284	16.71	17.48	23.08	37.13	HET
10 02 25.85+61 08 58.1	19.34	2.32	0.96	0.38	0.18	0.08	-448	-328	6	DC	3581	16.33	17.20	27.79	73.15	MMT
10 05 21.05+53 54 08.4	18.02	0.50	0.24	0.05	-0.02	0.04	-145	-219	6	DA	6800	13.52	13.85	68.91	85.79	2.7m
10 11 05.63+00 29 44.4	17.23	0.69	0.31	0.11	-0.02	0.18	-219	55	6	DAH	6184	13.93	14.32	40.48	43.33	2.7m
10 13 59.85+03 05 53.8	18.60	1.37	0.63	0.23	0.10	0.16	107	-101	6	DA	4964	14.90	15.60	42.00	29.29	MMT
10 14 14.45+04 01 37.4	16.76	0.46	0.11	0.01	-0.06	0.11	-199	26	6	DA	7506	13.08	13.40	48.78	46.41	2.7m
10 22 10.36+46 12 49.2	16.42	0.42	0.20	0.05	-0.06	0.07	9	-121	6	DA	6993	13.39	13.72	35.38	20.35	2.7m
10 23 56.10+63 48 33.8	18.08	0.86	0.34	0.09	0.00	0.05	-344	-216	6	DA	6243	13.89	14.28	58.47	112.58	2.7m
10 48 01.84+63 34 48.9	17.90	1.43	0.61	0.29	0.02	0.04	-258	-142	6	DA	5004	14.87	15.55	29.94	41.79	MMT
11 02 13.70+67 07 52.6	19.55	1.74	0.65	0.29	0.03	0.09	-380	-185	6	DC	4840	15.01	15.76	59.24	118.67	HET
11 07 31.38+48 55 23.0	19.39	2.02	0.92	0.30	0.12	0.11	-726	-79	6	DC	4020	15.82	16.77	34.85	120.64	HET
11 11 54.54+03 37 26.2	18.22	0.91	0.37	0.11	0.06	0.21	-371	-127	6	DA	5899	14.14	14.57	57.72	107.28	2.7m
11 13 06.26+00 32 43.7	17.60	0.53	0.21	-0.07	-0.04	0.34	-363	-89	6	DC	6953	13.42	13.75	65.60	116.21	2.7m
11 15 36.96+00 33 17.3	17.75	1.52	0.66	0.24	0.05	0.23	37	-250	6	DA	4816	15.04	15.79	26.57	31.83	MMT
11 19 40.62-01 07 55.1	19.79	2.01	0.85	0.24	0.15	0.23	-291	-28	6	DC	4283	15.55	16.47	49.77	68.97	HET
11 36 55.18+04 09 52.6	16.98	0.45	-0.10	0.32	0.51	0.12	-96	-53	4	DA	10077	11.79	12.18	95.28	49.52	2.7m
11 43 52.16-01 31 49.4	17.36	0.72	0.24	0.09	-0.02	0.10	-277	-2	6	DA	6594	13.65	14.00	48.57	63.78	2.7m
11 44 39.54+66 29 28.5	17.47	0.62	0.22	0.04	-0.06	0.05	-145	-20	6	DAH	6919	13.44	13.77	55.76	38.68	2.7m
11 46 25.77-01 36 36.9	16.48	0.59	0.25	0.12	-0.06	0.07	358	-434	6	DA	6516	13.70	14.05	31.35	83.61	2.7m

Table 1—Continued

Name (SDSS J)	$g$	$u - g$	$g - r$	$r - i$	$i - z$	$A_u$	$\mu_{ra}$	$\mu_{dec}$	Ep	Type	$T_{\text{eff}}$	$M_{\text{bol}}$	$M_g$	D	$V_T$	Source
12 02 00.48−03 13 47.4	19.86	2.37	0.85	0.32	0.06	0.15	−73	134	6	DC	4151	15.69	16.62	47.03	34.01	MMT
12 03 28.65+04 26 53.4	18.11	1.36	0.66	0.28	0.08	0.10	−252	156	6	DC	4852	15.00	15.75	30.66	43.07	MMT
12 04 39.54+62 22 16.4	19.16	1.69	0.78	0.29	0.10	0.10	−21	−159	6	DC	4528	15.31	16.17	40.92	31.11	MMT
12 05 29.15+04 49 35.6	18.45	0.89	0.48	0.19	0.07	0.09	−138	−53	6	DC	5524	14.43	14.94	51.65	36.19	MMT
12 33 22.45+06 07 10.7	18.21	1.32	0.55	0.19	0.03	0.09	−79	−352	6	DA	5302	14.61	15.19	41.41	70.80	2.7m
12 34 08.12+01 09 47.4	19.73	1.40	0.54	0.25	0.03	0.13	−284	−55	6	DA	5177	14.72	15.34	79.01	108.34	HET
12 38 47.85+51 22 07.4	17.32	0.46	0.12	−0.02	−0.13	0.07	−319	−21	6	DA	7710	12.96	13.29	65.38	99.06	2.7m
13 00 21.25+01 30 45.5	17.74	1.23	0.54	0.18	0.12	0.10	−374	145	6	DA	5297	14.61	15.20	33.48	63.66	2.7m
13 01 21.14+67 13 07.4	16.69	0.56	0.25	0.09	−0.04	0.06	151	52	4	DA	6629	13.63	13.97	35.51	26.88	2.7m
13 03 13.03−03 23 23.9	16.81	0.45	0.16	0.02	−0.09	0.13	32	−137	6	DA	7160	13.29	13.62	45.47	30.32	2.7m
13 13 13.12+02 26 45.8	18.84	2.04	1.07	0.37	0.18	0.14	−744	−116	6	DC	3394	16.56	17.38	20.23	72.21	MMT
13 22 54.60−00 50 42.8	18.82	1.75	0.76	0.31	0.09	0.14	−156	118	6	DC	4505	15.33	16.20	35.08	32.52	MMT
13 36 16.05+00 17 32.7	17.34	0.51	0.36	0.76	0.58	0.12	−278	−141	6	DA+M	6116	13.98	14.38	40.76	60.23	2.7m
13 39 39.55+67 04 49.8	19.79	0.75	0.28	0.12	−0.02	0.07	−194	235	5	DA	6409	13.78	14.14	137.61	198.77	HET
13 40 43.35+02 03 48.3	18.01	1.11	0.43	0.20	0.04	0.13	−534	28	6	DC	5600	14.37	14.87	44.45	112.66	2.7m
13 57 58.43+60 28 55.3	18.04	0.72	0.35	0.11	−0.05	0.07	−304	55	6	DC	6186	13.93	14.32	56.53	82.78	2.7m
14 22 25.73+04 59 39.7	19.34	1.54	0.83	0.30	0.08	0.15	−277	−62	6	DC	4365	15.47	16.37	41.08	55.27	HET
14 26 59.40+49 21 00.6	16.93	0.55	0.18	0.07	−0.09	0.11	−96	44	6	DC	6927	13.43	13.77	44.52	22.28	2.7m
14 52 24.95−00 11 34.7	18.25	1.36	0.58	0.20	0.07	0.27	155	129	6	DC	5052	14.83	15.49	38.98	37.26	2.7m
15 48 35.89+57 08 26.4	17.70	0.80	0.39	0.13	0.05	0.06	−220	−138	6	DC	5975	14.08	14.50	44.38	54.64	2.7m
15 55 34.18+50 25 47.8	16.70	0.75	0.31	0.13	0.00	0.10	−234	−5	6	DA	6204	13.92	14.31	31.13	34.54	2.7m
16 09 20.13+52 22 39.6	18.21	0.65	0.25	0.12	0.01	0.10	155	281	6	DA	6467	13.73	14.09	68.91	104.82	2.7m
16 15 44.67+44 49 42.5	19.56	1.63	0.75	0.27	0.08	0.05	44	−237	6	DC	4698	15.14	15.95	53.41	61.02	HET
16 23 24.05+34 36 47.7	17.18	0.39	0.11	0.08	0.45	0.10	−58	105	6	DA	7650	13.00	13.32	61.11	34.74	2.7m
16 27 12.99+00 28 18.6	17.38	0.78	0.31	0.06	−0.01	0.47	−194	−73	6	DA	5983	14.08	14.49	44.31	43.54	2.7m
16 27 31.09+48 59 19.0	19.19	1.51	0.59	0.24	0.05	0.07	−91	77	6	DZA	5105	14.78	15.43	58.01	32.78	MMT
16 48 47.07+39 39 17.0	18.81	1.29	0.54	0.16	0.06	0.07	−126	0	6	DC	5401	14.53	15.08	56.98	34.03	MMT
16 54 45.70+38 29 36.6	16.93	0.96	0.40	0.15	0.02	0.08	18	−325	5	DZA	5847	14.18	14.62	29.72	45.85	2.7m
16 59 40.00+32 03 20.1	17.56	0.63	0.28	0.07	0.01	0.16	−238	−244	6	DA	6428	13.76	14.12	51.35	82.96	2.7m
17 04 47.70+36 08 47.4	18.63	1.79	0.75	0.28	0.12	0.13	186	−175	6	DC	4560	15.28	16.13	33.21	40.20	HET
17 14 33.26+27 38 36.1	18.16	0.40	0.12	0.01	−0.11	0.24	49	−20	6	DC	7235	13.24	13.57	89.96	22.57	2.7m
17 22 57.78+57 52 50.7	19.17	1.14	0.46	0.23	0.06	0.15	−37	390	6	DC	5403	14.53	15.08	69.64	129.32	HET
17 24 13.32+27 56 55.2	17.47	0.78	0.30	0.11	0.00	0.26	47	−60	6	DA	6131	13.97	14.37	45.61	16.48	2.7m
17 28 07.29+26 46 20.1	18.02	0.97	0.42	0.16	0.04	0.23	−45	−255	6	DA	5619	14.36	14.85	46.57	57.15	2.7m
20 41 28.99−05 20 27.7	19.09	1.65	0.70	0.26	0.06	0.26	−149	−29	6	DC	4673	15.17	15.98	45.68	32.87	MMT
20 42 59.23+00 31 56.6	19.67	1.65	0.81	0.30	0.07	0.37	−71	−244	6	DC	4201	15.63	16.57	47.29	56.96	HET
20 45 06.97+00 37 34.4	19.43	0.59	0.25	0.12	0.00	0.45	32	−32	6	DA	6093	14.00	14.40	117.73	25.25	MMT
20 45 57.53−07 10 03.5	19.08	1.61	0.68	0.21	0.12	0.39	−73	−134	6	DC	4682	15.16	15.97	47.90	34.65	MMT
21 03 30.85−00 24 46.4	18.22	0.66	0.27	0.07	0.02	0.34	61	−139	6	DC	6223	13.91	14.29	68.61	49.36	MMT
21 16 40.30−07 24 52.7	17.93	1.67	0.69	0.25	0.05	0.70	111	−223	6	DC	4359	15.47	16.38	25.89	30.56	2.7m
21 18 05.21−07 37 29.1	19.85	2.42	0.98	0.33	0.11	1.17	115	−144	5	DC	3401	16.55	17.37	43.44	37.95	HET
21 18 58.65+11 20 17.7	18.13	0.77	0.27	0.09	0.01	0.42	359	−13	5	DA	6086	14.00	14.40	64.24	109.38	2.7m
21 25 01.48−07 34 56.0	19.48	0.74	0.26	0.08	0.01	0.56	64	13	5	DA	6063	14.02	14.42	122.54	37.93	MMT
21 36 43.08−07 06 38.2	19.43	0.60	0.25	0.08	−0.03	0.20	69	−11	5	DA	6520	13.70	14.05	125.93	41.71	MMT
21 47 52.10−08 24 36.8	17.59	0.75	0.32	0.14	−0.01	0.24	30	153	6	DA	6010	14.06	14.47	45.77	33.82	2.7m
21 54 30.69+13 00 26.7	18.75	1.55	0.61	0.25	0.10	0.41	367	−73	6	DZA	4768	15.08	15.86	43.76	77.62	MMT
21 55 01.53+12 01 16.4	18.47	0.65	0.25	0.07	−0.06	0.54	−76	−25	4	DA	6121	13.98	14.37	79.14	30.01	MMT
22 04 14.16−01 09 31.2	19.88	1.88	0.83	0.24	0.11	0.44	112	−303	6	DC	4189	15.65	16.58	52.87	80.95	HET
22 22 33.90+12 21 43.0	19.13	1.95	1.02	0.36	0.18	0.41	731	198	4	DC	3448	16.49	17.33	25.78	92.53	HET
22 41 57.63+13 32 38.8	17.36	0.82	0.35	0.10	0.02	0.26	61	−395	6	DA	5986	14.07	14.49	40.90	77.49	2.7m
22 42 06.19+00 48 22.8	19.38	2.43	0.91	0.34	0.08	0.36	132	−76	6	DC	3407	16.55	17.37	29.12	21.02	HET

Table 1—Continued

Name (SDSS J)	$g$	$u - g$	$g - r$	$r - i$	$i - z$	$A_u$	$\mu_{ra}$	$\mu_{dec}$	Ep	Type	$T_{\text{eff}}$	$M_{\text{bol}}$	$M_g$	D	$V_T$	Source
22 54 08.64+13 23 57.2	19.33	2.04	0.97	0.33	0.10	0.26	329	-199	6	DC	3356	16.61	17.41	26.72	48.71	HET
23 12 06.08+13 10 57.6	17.45	1.38	0.56	0.16	0.08	0.38	-132	-256	6	DA	5078	14.80	15.46	28.40	38.78	2.7m
23 25 19.89+14 03 39.7	16.30	1.55	0.57	0.27	0.09	0.23	336	115	6	DC	4941	14.92	15.63	14.80	24.92	2.7m
23 30 40.47+01 00 47.4	17.36	0.64	0.17	0.06	0.02	0.20	-255	-125	6	DA	6768	13.54	13.88	53.63	72.19	2.7m
23 30 55.20+00 28 52.3	19.77	1.96	0.89	0.30	0.11	0.17	151	91	6	DC	4126	15.71	16.65	44.42	37.12	HET
23 37 07.68+00 32 42.3	18.13	1.01	0.45	0.14	-0.02	0.18	305	162	6	DA	5629	14.35	14.84	48.35	79.15	2.7m
23 40 41.47-11 06 36.9	18.46	0.53	0.25	0.74	0.85	0.15	19	-87	6	DA+M	6612	13.64	13.99	82.58	34.86	MMT
23 42 45.75-10 01 21.4	18.83	1.52	0.71	0.26	0.04	0.16	-28	-95	6	DA	4719	15.12	15.92	40.18	18.86	MMT
23 50 42.52-08 46 18.9	19.03	1.04	0.50	0.22	0.08	0.18	209	-139	6	DA	5298	14.61	15.20	62.18	73.97	HET
23 54 16.59+00 30 01.2	19.25	0.71	0.20	0.10	0.04	0.20	53	18	5	DA	6568	13.67	14.02	119.10	31.60	MMT

Table 2. Spectroscopically Identified Subdwarf Stars

Name (SDSS J)	$g$	$u - g$	$g - r$	$r - i$	$i - z$	$A_u$	$\mu_{ra}$	$\mu_{dec}$	Ep	Dist22	Source
00 18 13.74–08 54 58.6	19.48	0.73	0.24	0.07	–0.03	0.23	–41	–33	5	15.1	MMT
00 29 58.84+15 18 41.1	19.20	0.84	0.29	0.08	0.07	0.34	–46	–31	4	30.4	MMT
00 53 31.26+00 05 09.8	19.38	2.18	1.09	0.53	0.23	0.13	137	–22	6	24.4	MMT
01 05 02.05+14 01 54.4	19.40	1.00	0.43	0.15	0.08	0.37	–11	48	5	25.4	MMT
01 31 19.61+00 02 57.6	17.93	2.18	1.14	0.45	0.25	0.17	230	–115	6	31.0	2.7m
01 48 33.19–01 10 43.3	17.98	1.91	0.85	0.36	0.15	0.17	152	–106	6	13.8	2.7m
01 56 32.67+14 47 29.7	17.48	1.52	0.66	0.27	0.07	0.29	111	–95	5	7.8	2.7m
02 12 13.80+00 00 42.1	18.81	1.33	0.51	0.21	0.10	0.16	81	61	5	12.9	MMT
02 29 47.61–08 50 20.2	16.80	1.62	0.74	0.24	0.14	0.17	151	–95	6	6.4	2.7m
02 38 07.99–09 30 33.6	18.61	1.87	0.77	0.30	0.19	0.15	80	–46	6	29.4	MMT
03 00 48.83–00 44 08.0	17.21	1.20	0.60	0.26	0.19	0.60	83	–113	6	12.6	2.7m
03 07 22.43+00 34 05.2	15.68	1.18	0.49	0.18	0.08	0.55	156	–109	6	41.2	2.7m
03 10 43.74–08 18 48.7	17.49	0.86	0.25	0.08	0.03	0.36	–32	48	5	13.4	2.7m
03 18 45.08–06 12 36.3	16.56	1.51	0.73	0.28	0.18	0.33	159	–104	6	35.0	2.7m
03 51 47.74–05 33 02.9	15.94	1.54	0.74	0.28	0.12	0.56	237	–264	6	31.9	2.7m
07 36 36.05+29 02 22.7	17.41	1.11	0.34	0.13	0.05	0.24	–18	–71	5	4.6	2.7m
07 38 56.39+32 25 18.9	17.52	1.73	0.80	0.33	0.16	0.22	5	–144	6	17.0	2.7m
07 52 17.25+25 21 55.6	16.79	1.03	0.27	0.07	0.00	0.40	146	214	4	26.2	2.7m
08 00 05.13+46 08 01.1	16.64	1.13	0.55	0.16	0.11	0.38	–2	309	4	19.6	2.7m
08 13 06.76+02 34 25.9	17.15	1.30	0.45	0.19	0.09	0.14	309	–45	5	7.7	2.7m
08 30 49.85+02 50 18.6	18.24	1.55	0.53	0.12	0.12	0.17	45	87	6	5.5	2.7m
08 37 43.43+02 01 01.7	17.91	2.14	0.78	0.30	0.11	0.25	–15	–443	4	5.5	MMT
09 05 13.97+47 37 28.5	18.67	2.79	1.33	0.51	0.31	0.08	–159	–344	6	35.1	MMT
09 19 09.52+56 41 00.1	17.03	2.09	0.70	0.24	0.14	0.17	1	–263	5	10.0	2.7m
09 35 59.33+60 13 23.0	17.22	1.40	0.55	0.25	0.09	0.15	–4	–275	4	11.3	2.7m
09 59 26.92–00 08 49.7	16.82	2.03	0.79	0.31	0.09	0.16	–315	90	5	6.0	2.7m
10 05 37.72+52 59 13.2	17.30	0.95	0.24	0.08	–0.01	0.04	–3	131	5	12.1	2.7m
10 06 33.59–00 27 32.4	17.95	1.01	0.47	0.16	0.08	0.19	–237	–72	5	4.1	2.7m
10 17 39.82+02 09 33.8	16.79	1.40	0.59	0.21	0.12	0.25	–240	190	4	16.5	2.7m
10 41 49.72+62 44 55.6	16.69	0.98	0.29	0.08	0.05	0.03	55	161	5	12.2	2.7m
10 51 57.48+02 03 00.4	19.74	1.97	1.05	0.46	0.28	0.22	166	–105	5	32.0	MMT
11 07 23.94+62 26 06.0	16.29	0.97	0.33	0.11	0.03	0.05	46	239	4	25.4	2.7m
11 13 27.37+58 58 48.5	17.09	2.32	1.24	0.48	0.31	0.05	–296	–472	6	59.0	2.7m
11 22 04.68+65 53 59.7	17.54	1.08	0.36	0.17	0.04	0.06	–63	–152	5	39.5	2.7m
11 31 02.89+66 57 51.2	16.66	1.64	0.52	0.25	0.11	0.05	–116	206	5	42.9	2.7m
11 35 12.08+03 28 41.2	19.24	2.80	1.18	0.47	0.31	0.11	–163	–255	6	20.1	MMT
11 52 06.86+67 02 04.2	16.33	0.87	0.21	0.08	0.02	0.06	–117	143	4	19.8	2.7m
12 09 45.96+63 02 43.9	16.96	0.86	0.25	0.08	0.01	0.10	–71	196	5	26.5	2.7m
12 50 47.35+03 26 52.8	18.28	2.17	0.98	0.43	0.19	0.16	–97	–221	4	12.5	2.7m
12 52 26.29+02 28 38.8	16.78	1.44	0.49	0.16	0.05	0.16	155	–100	5	19.1	2.7m
13 05 07.26+04 14 08.1	16.81	0.92	0.32	0.12	0.02	0.13	–135	–47	5	9.3	2.7m
13 42 33.44+58 00 19.7	17.16	1.08	0.32	0.13	0.04	0.04	15	196	5	15.7	2.7m
14 06 35.95+61 53 35.6	19.70	1.96	1.03	0.42	0.25	0.07	–84	296	5	36.2	HET
16 37 16.86+45 17 01.8	17.79	0.95	0.33	0.08	0.05	0.06	–83	–414	4	13.6	2.7m
17 02 06.35+31 47 49.9	17.71	1.57	0.58	0.19	0.13	0.21	246	–99	5	9.6	2.7m
17 17 37.03+62 34 48.1	18.26	1.10	0.32	0.16	0.00	0.12	–36	43	6	28.5	2.7m
17 19 18.54+29 15 38.6	17.52	1.55	0.59	0.14	0.08	0.20	72	142	5	11.1	2.7m
17 35 52.77+57 38 14.3	17.88	2.07	1.00	0.40	0.19	0.33	–89	156	6	20.0	2.7m
20 58 59.24–05 57 03.8	19.16	1.51	0.59	0.19	0.08	0.23	–51	51	4	12.1	MMT
21 34 27.61–08 15 11.0	18.41	1.34	0.49	0.15	0.08	0.18	–75	19	5	23.0	MMT
21 42 39.11–00 55 50.3	18.69	2.41	1.19	0.47	0.26	0.27	103	–173	6	13.6	MMT
21 48 19.02+00 39 43.2	18.30	0.99	0.35	0.10	0.01	0.81	–55	79	6	9.7	MMT
22 14 28.87+13 53 41.9	17.66	1.04	0.39	0.14	0.06	0.33	90	50	6	8.7	2.7m
22 54 49.68+12 59 22.6	19.23	1.75	1.00	0.31	0.21	0.20	226	–125	5	7.2	HET
22 58 03.60–10 07 02.0	19.33	2.73	1.08	0.57	0.29	0.20	108	–145	6	28.8	MMT

Note. — Proper motions for stars that have not been detected in 1 or 2 USNO-B epochs ( $E_p < 6$ ) or that have a neighbor brighter than 22 mag within 7 arcsec ( $Dist22 < 7$ ) are unreliable.

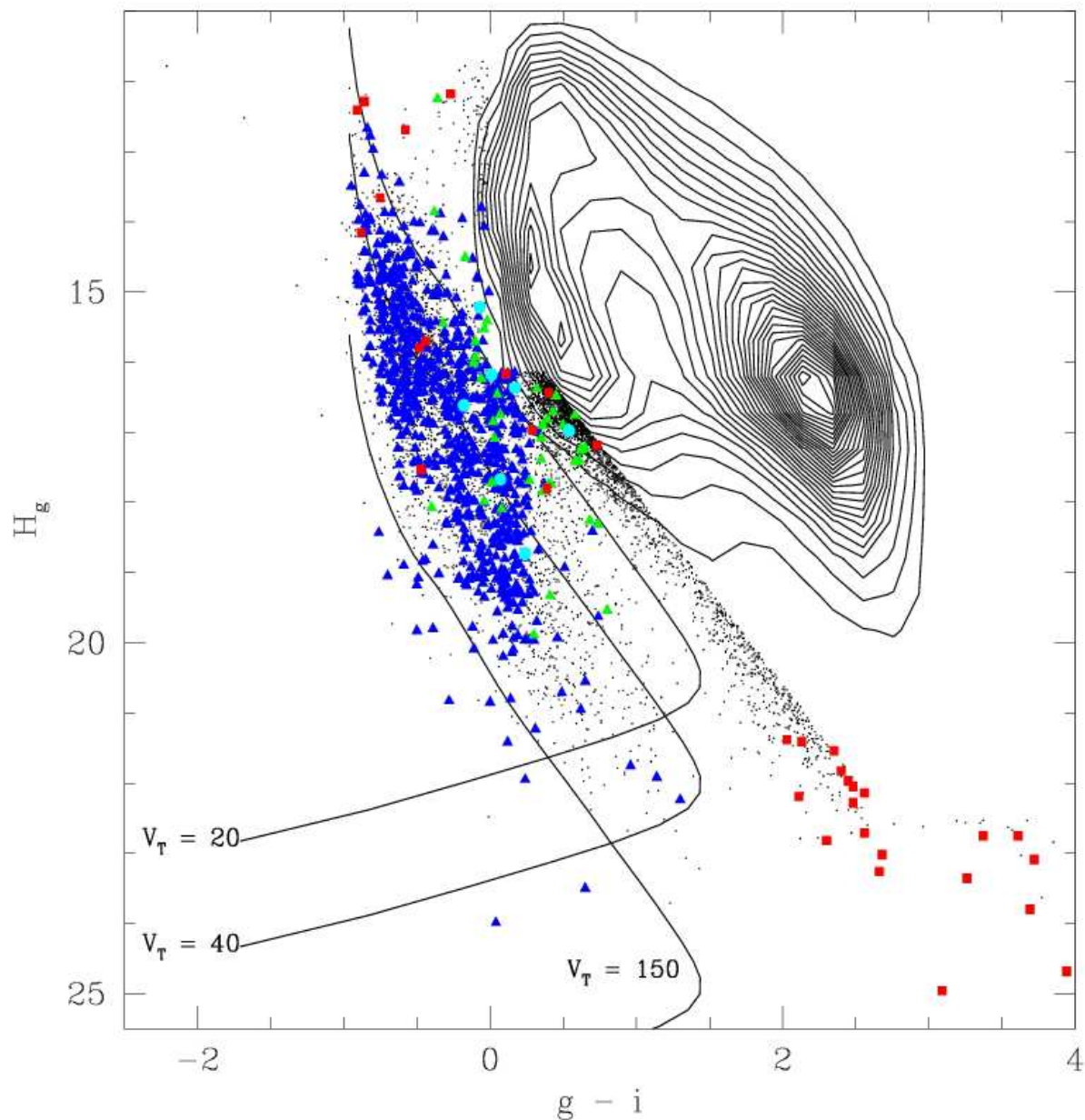


Fig. 1.— The reduced proper motion diagram for stars in the SDSS DR2. Individual stars are plotted only in the region of interest for white dwarfs, the remaining stars are represented by the contours. Previously known white dwarfs, white dwarf plus late type star binaries, subdwarfs, and quasars are shown as blue triangles, green triangles, red squares, and cyan circles, respectively. White dwarf cooling curves for different tangential velocities are shown as solid lines. The  $V_T = 20\text{--}40 \text{ km s}^{-1}$  curves mark the expected location of disk white dwarfs, whereas the  $V_T = 150 \text{ km s}^{-1}$  curve represents the halo white dwarfs.

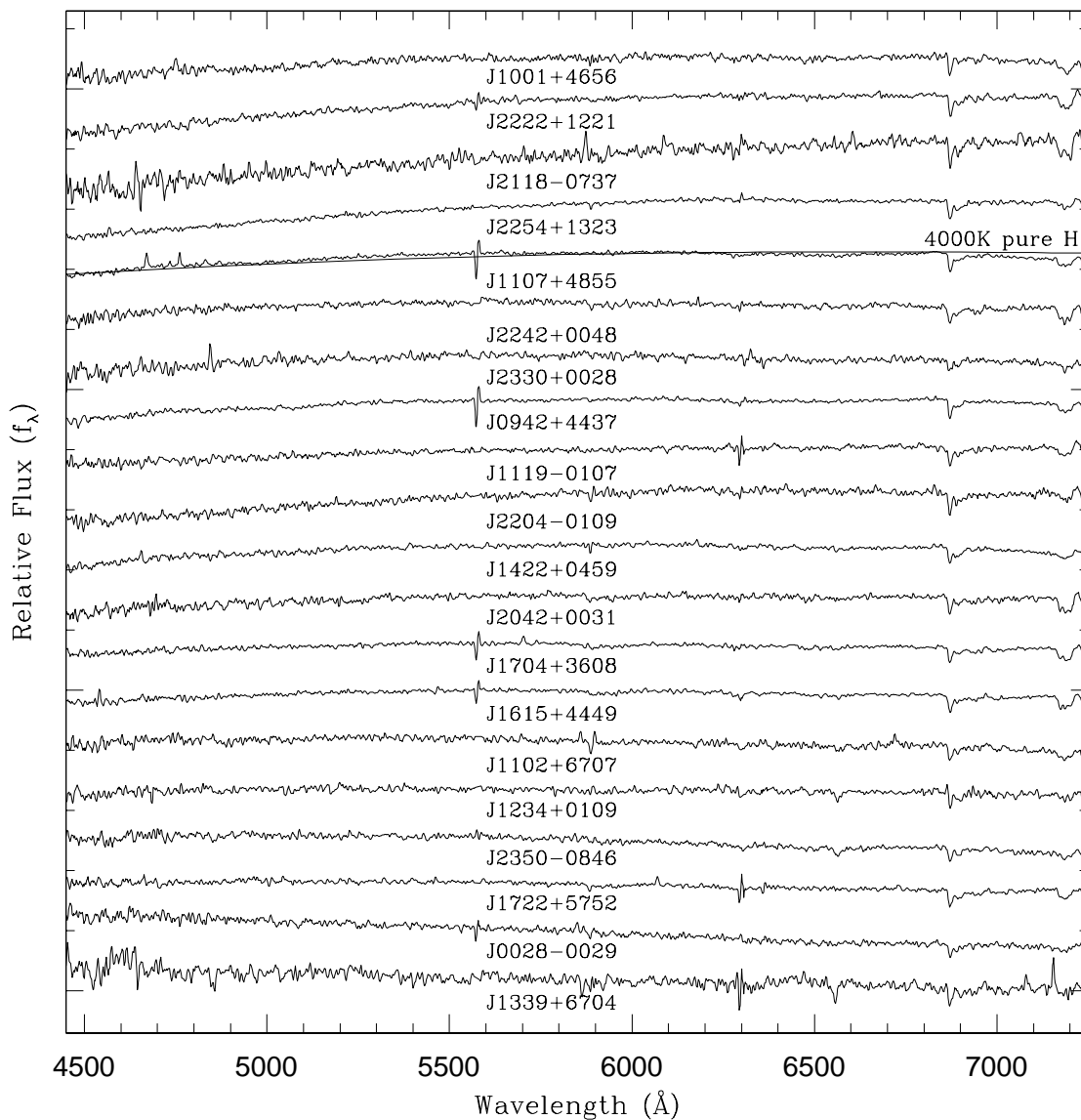


Fig. 2.— Optical spectra for white dwarfs observed at the Hobby–Eberly Telescope. The spectra are normalized at 5500 Å, and are shifted vertically from each other by arbitrary units. Synthetic spectrum of a 4000 K pure H atmosphere white dwarf (D. Saumon, private communication) is also shown. The  $g - r$  color increases from bottom to top.

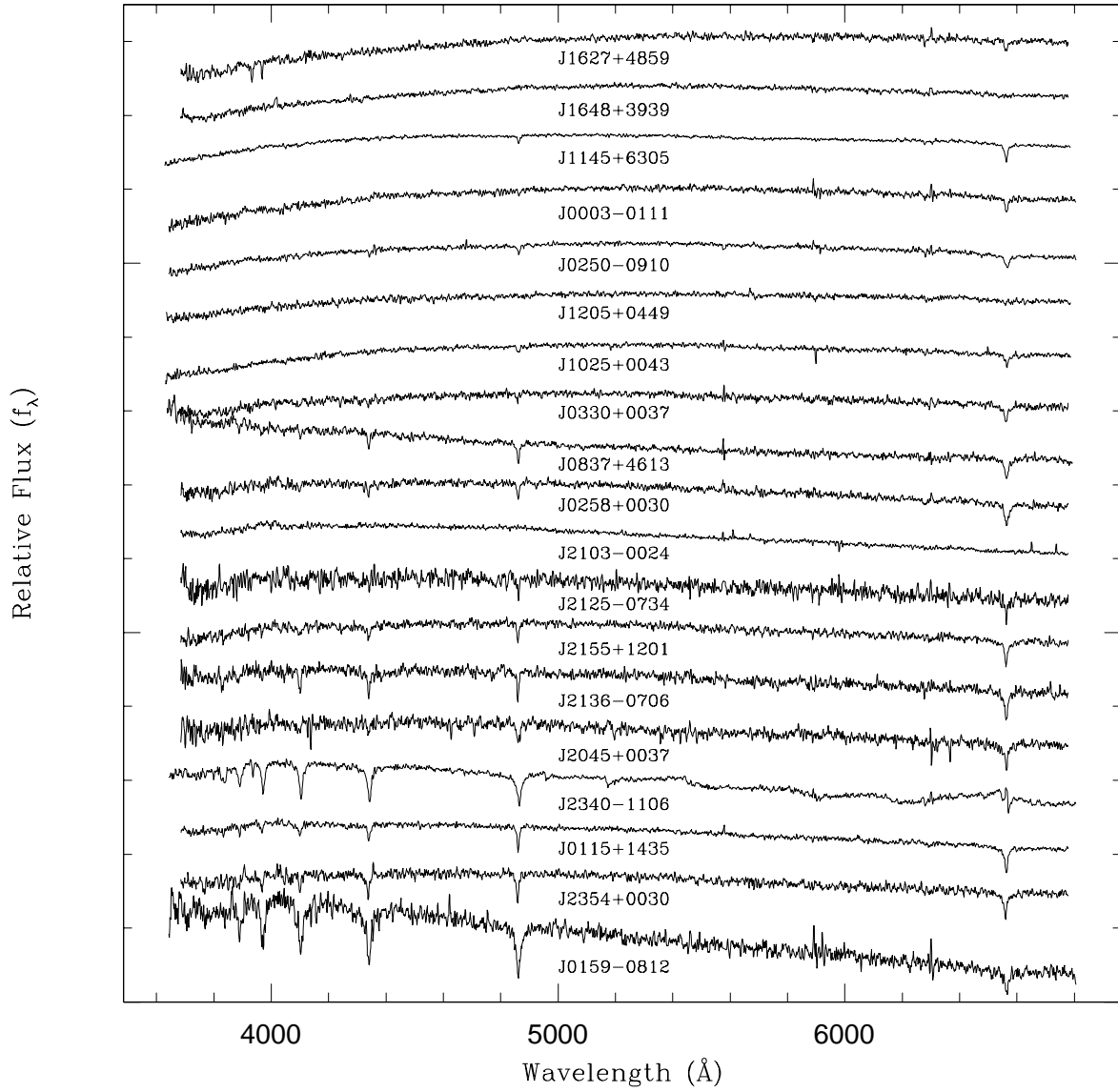


Fig. 3.— Same as figure 2, but for white dwarfs observed at the MMT.

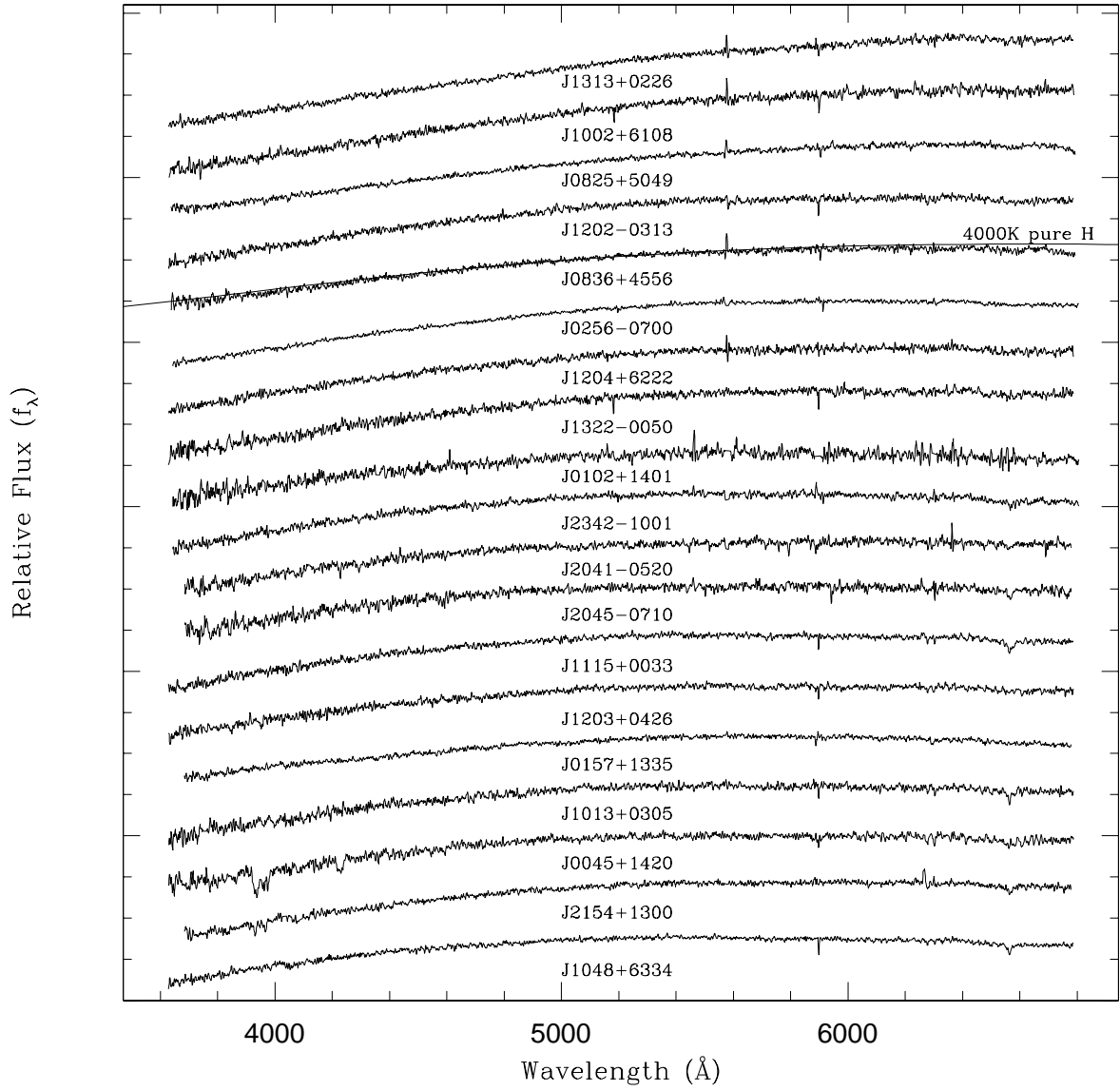


Figure 3b



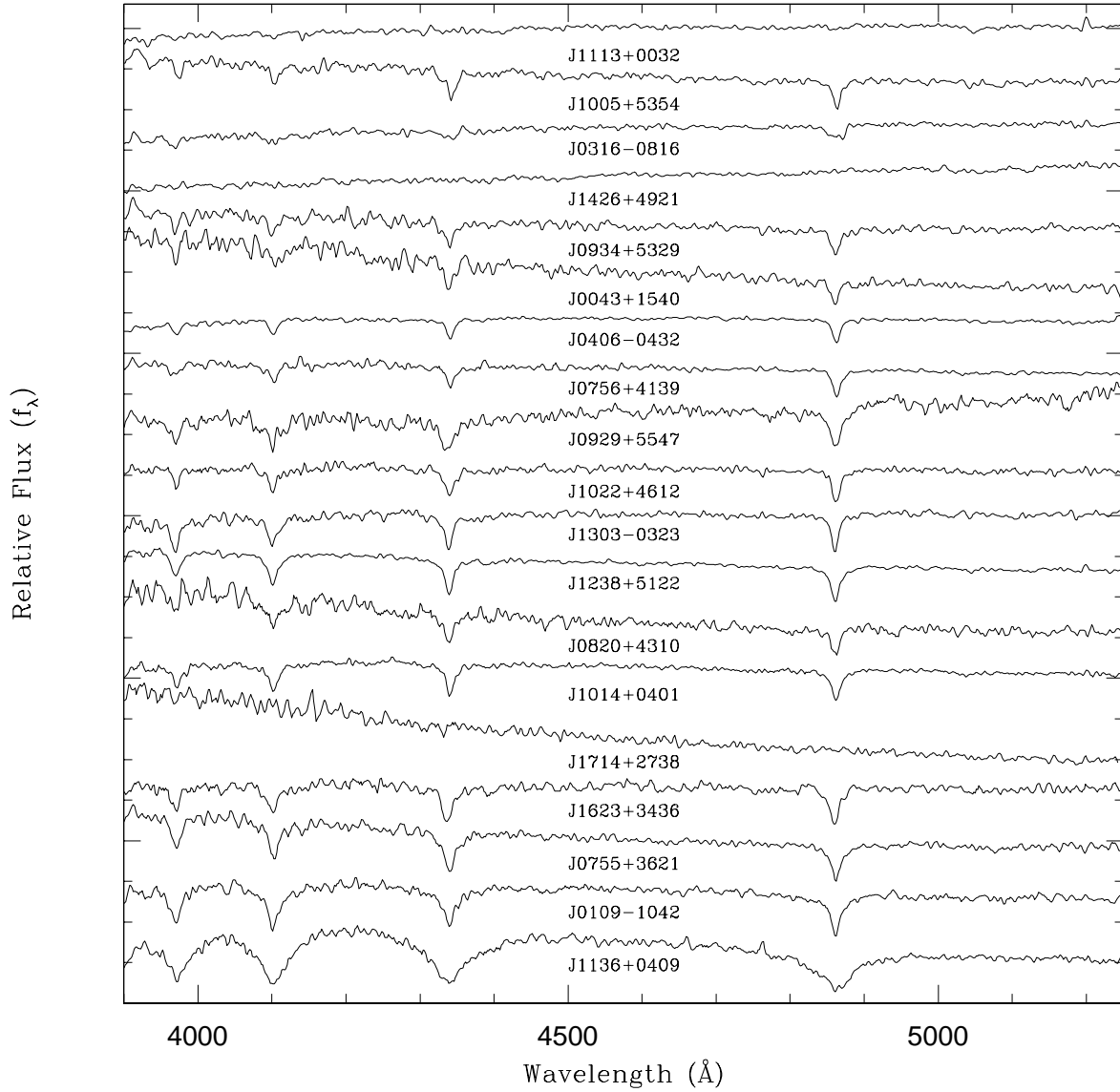


Fig. 4.— Optical spectra for white dwarfs observed at the McDonald 2.7m Harlan Smith Telescope. The spectra are normalized at 4600  $\text{\AA}$ , and are shifted vertically from each other by arbitrary units. The  $u - r$  color increases from bottom to top.

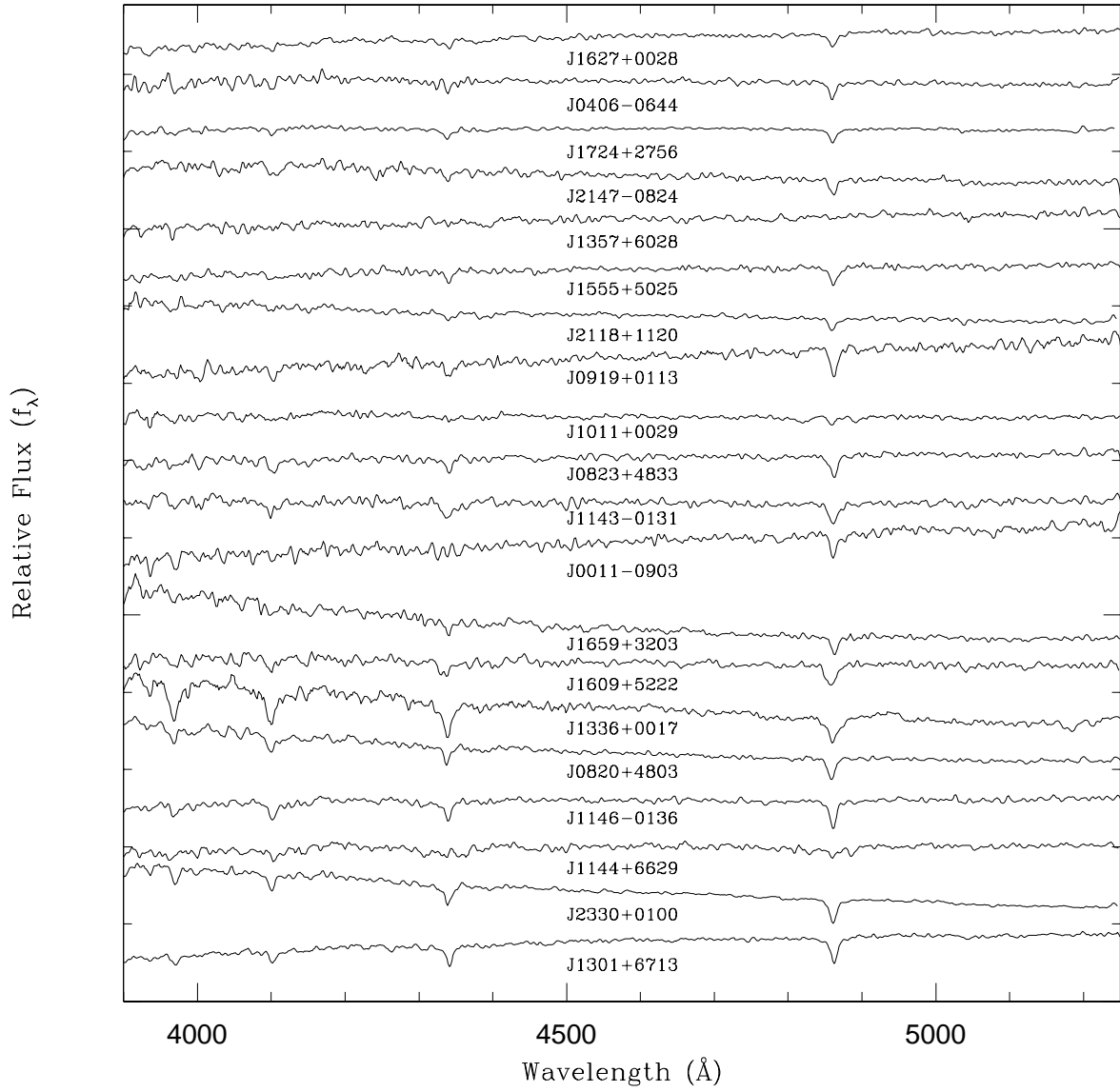


Figure 4b

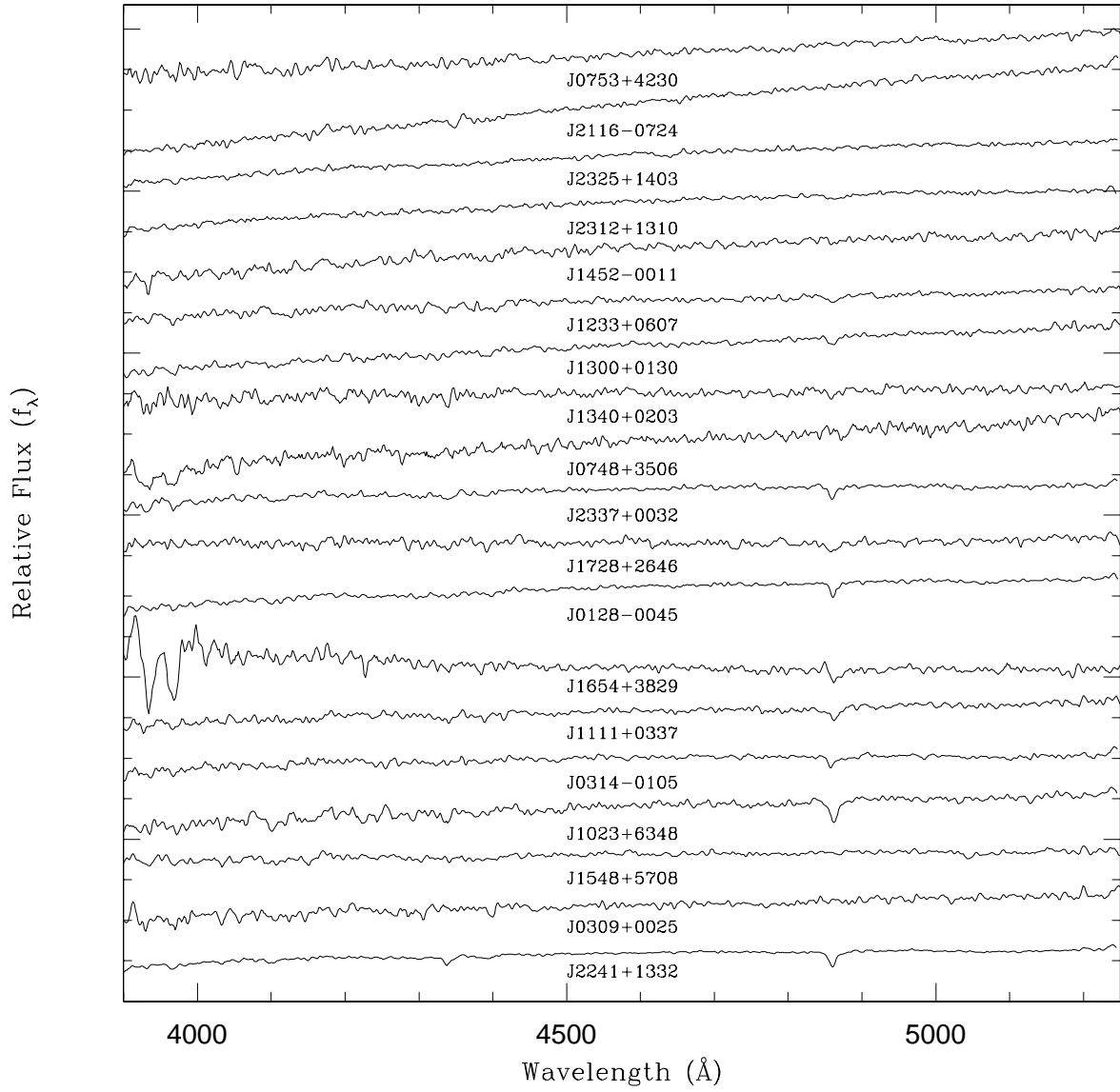


Figure 4c

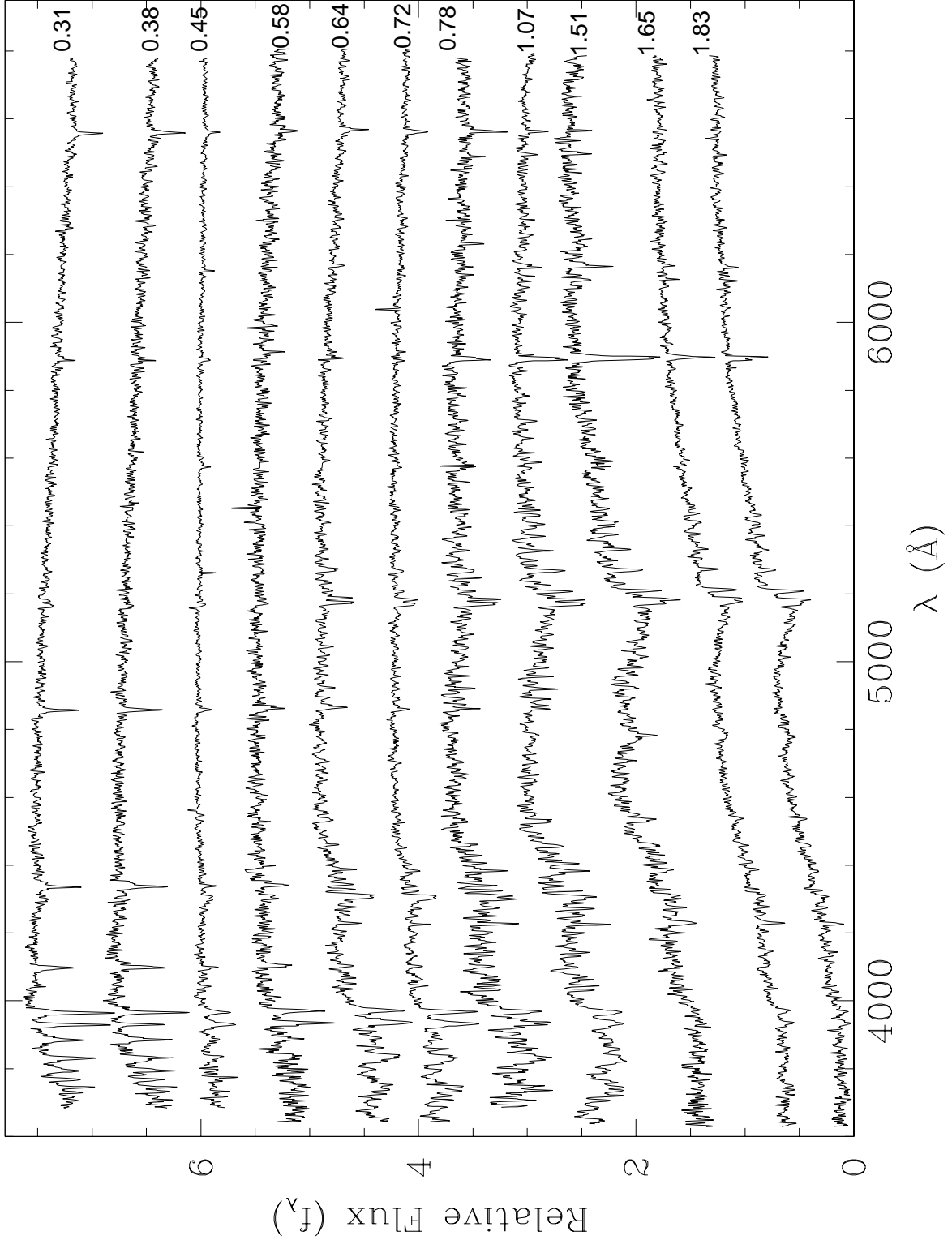


Fig. 5.— Optical spectra of several subdwarf stars observed at the MMT. The spectra are ordered in increasing  $g - i$  color, which is given on the right edge of each spectrum.

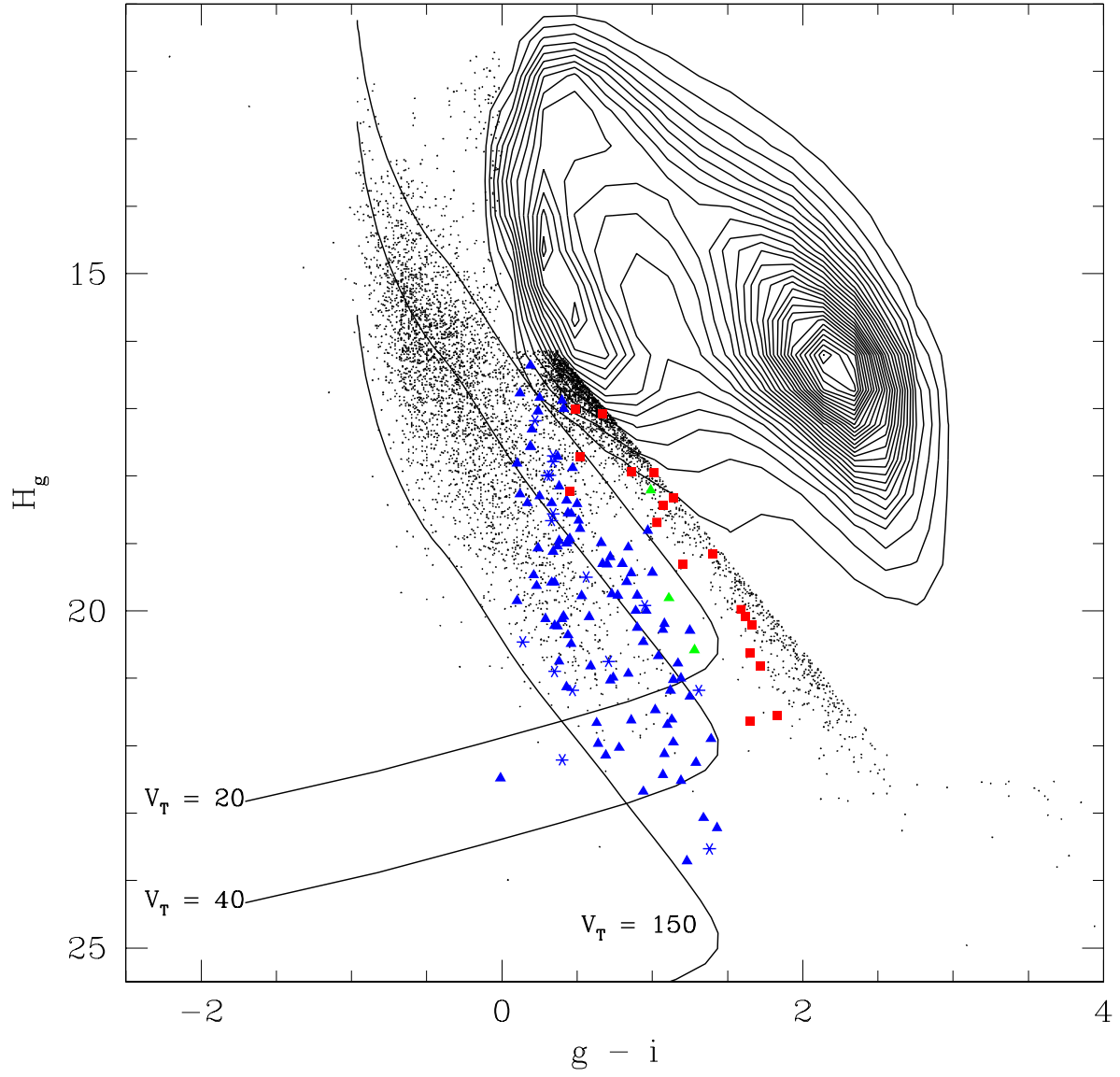


Fig. 6.— Same as figure 1, but for the spectroscopically confirmed white dwarfs, white dwarf + late type star binaries, subdwarfs, and quasars found in our study. White dwarfs that did not meet our criteria for reliable proper motions are plotted as blue asterisks.

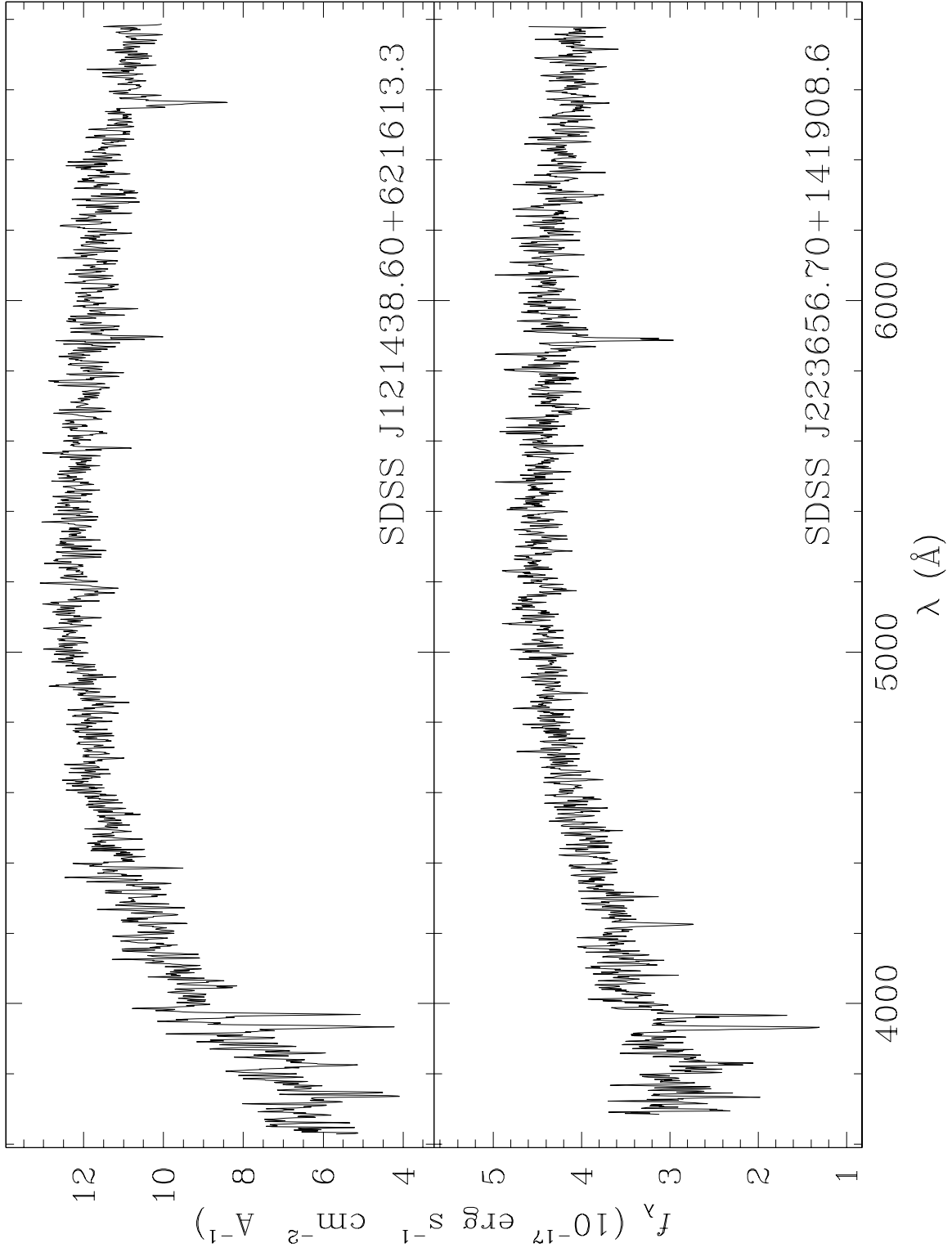


Fig. 7.— MMT spectra for two uncertain white dwarfs / subdwarfs.

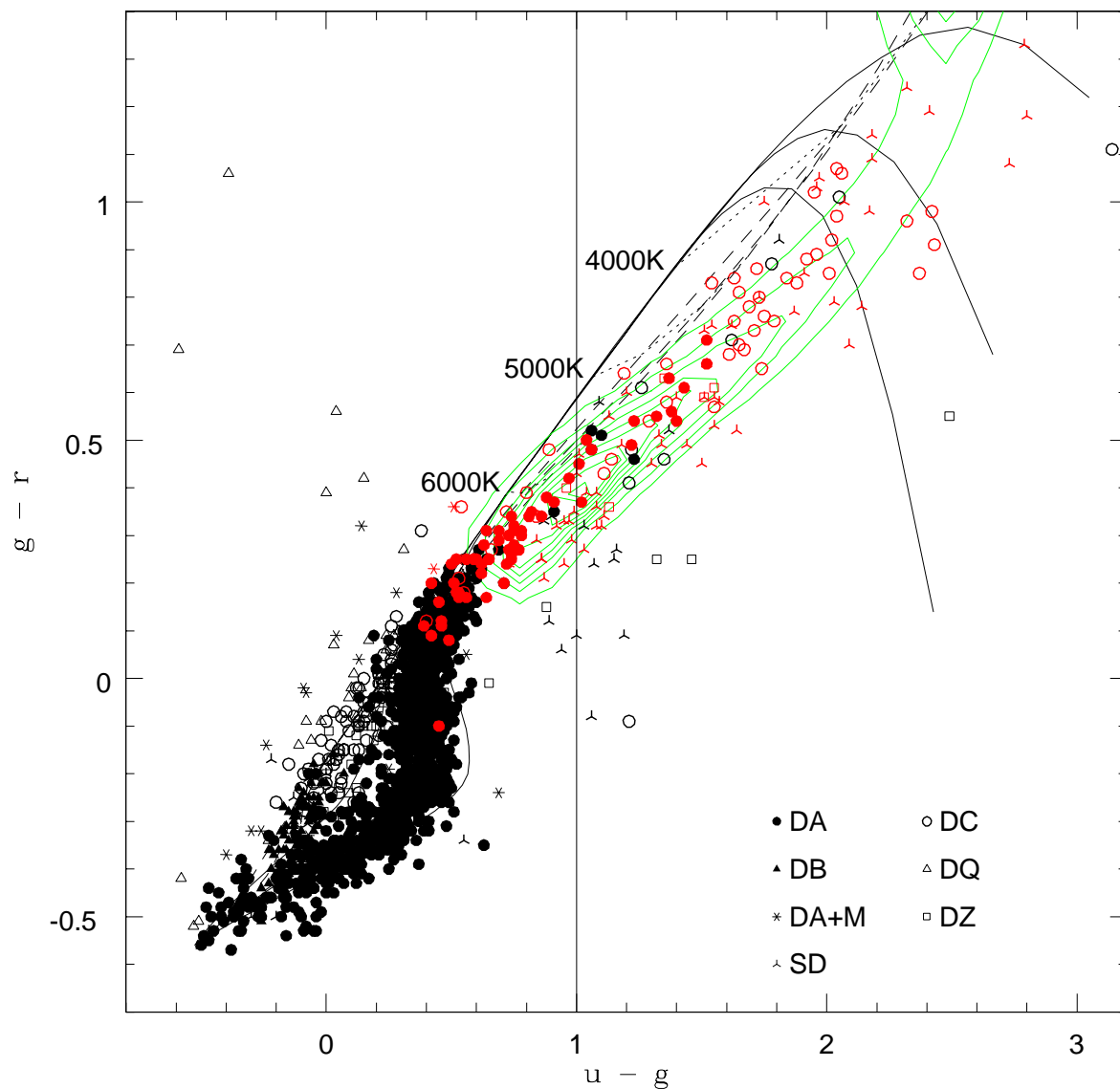


Fig. 8.— Color-color diagrams showing the white dwarfs and subdwarfs from our study (red symbols) and the literature (black symbols). Different types of white dwarfs are shown with different symbols. The contours represent objects without spectroscopic confirmation. The curves show the colors of white dwarf model atmospheres (P. Bergeron, private communication) of pure H (solid curves) and pure He (dashed curves) with  $\log g = 7, 8,$  and  $9$ , where the  $\log g = 9$  curve is the bottom and  $\log g = 7$  is the top curve in panel *a*. The dotted lines with labels connect models with the same effective temperature.

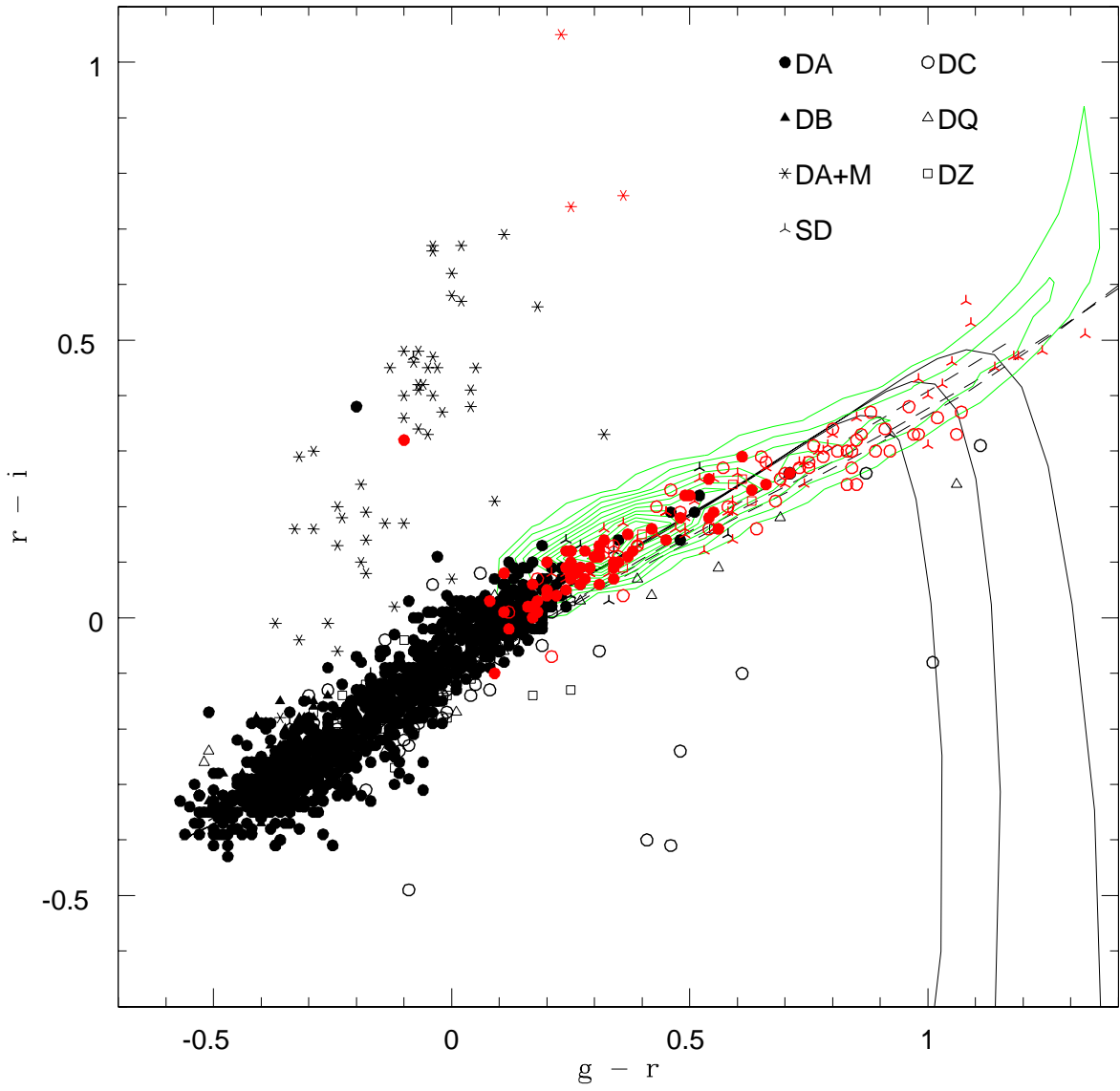


Figure 8b



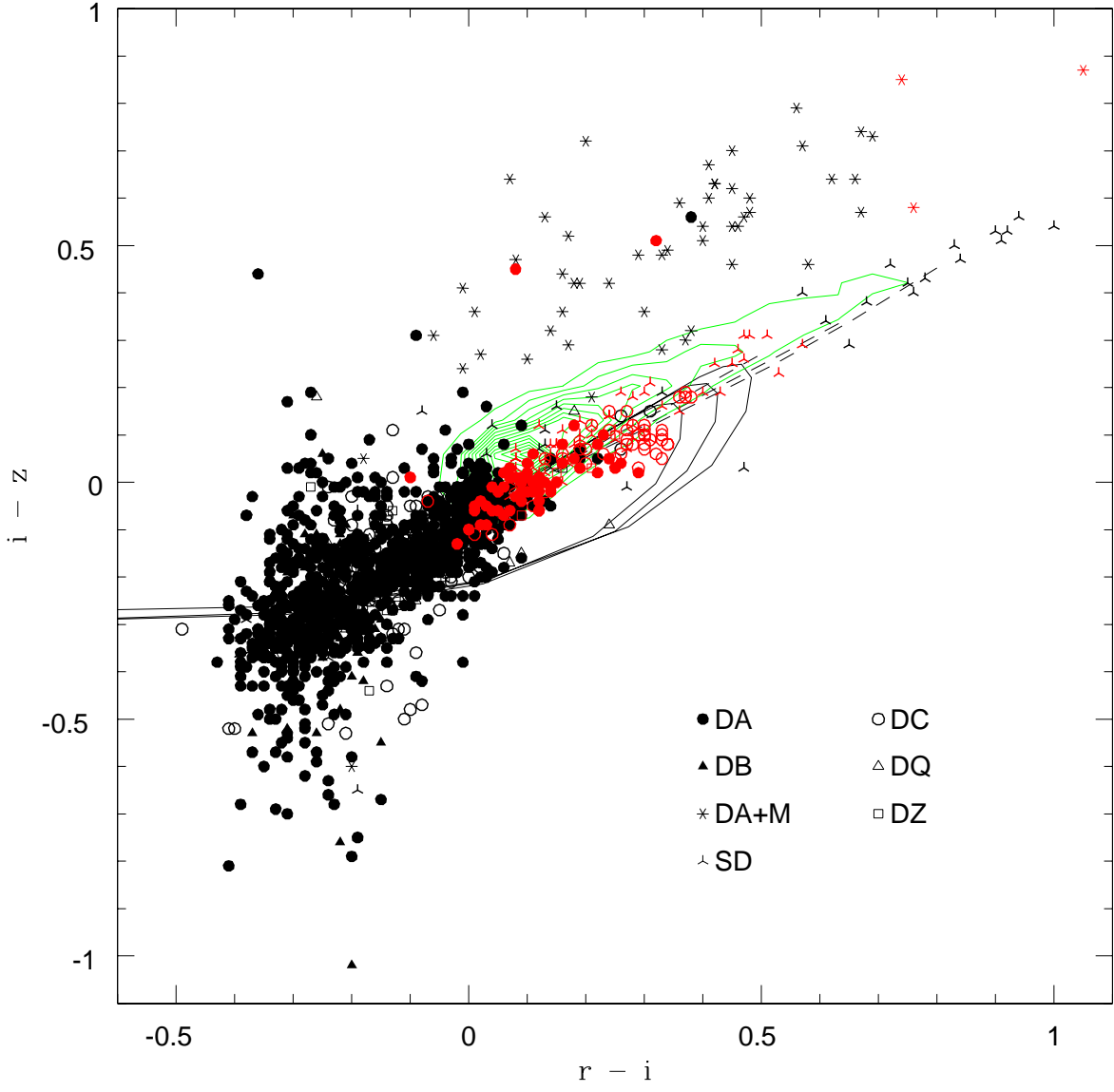


Figure 8c

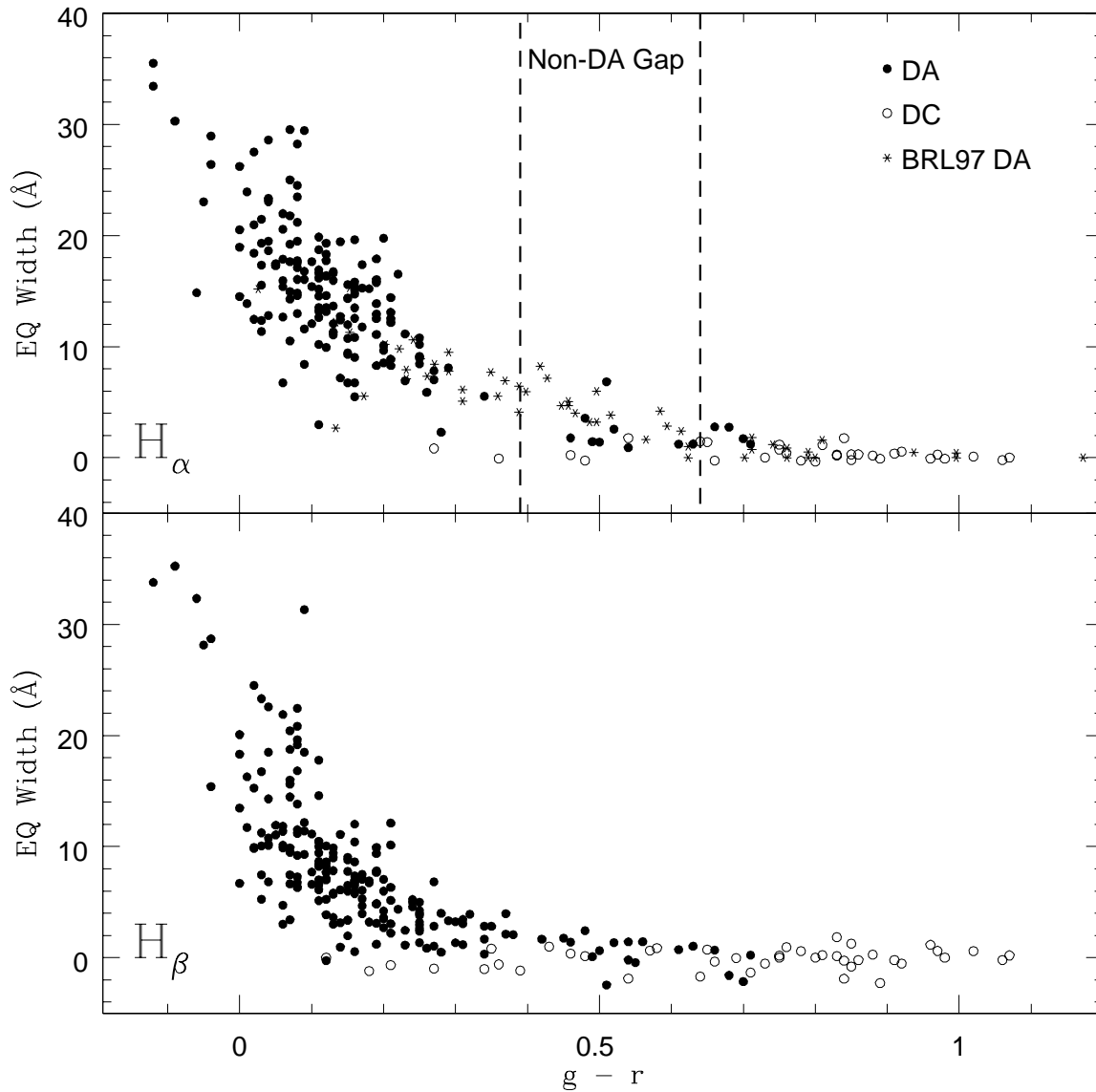


Fig. 9.— Equivalent width measurements of H $\alpha$  and H $\beta$  as a function of  $g - r$  for the DA and DC white dwarfs in our sample. The top panel also includes H $\alpha$  equivalent width measurements of the Bergeron, Ruiz & Leggett (1997) DA sample. The predicted non-DA gap for  $\log g = 8$  DA white dwarfs is marked by the dashed lines. Since McDonald 2.7m spectra do not cover H $\alpha$ , we do not have H $\alpha$  equivalent width measurements for some of our objects.

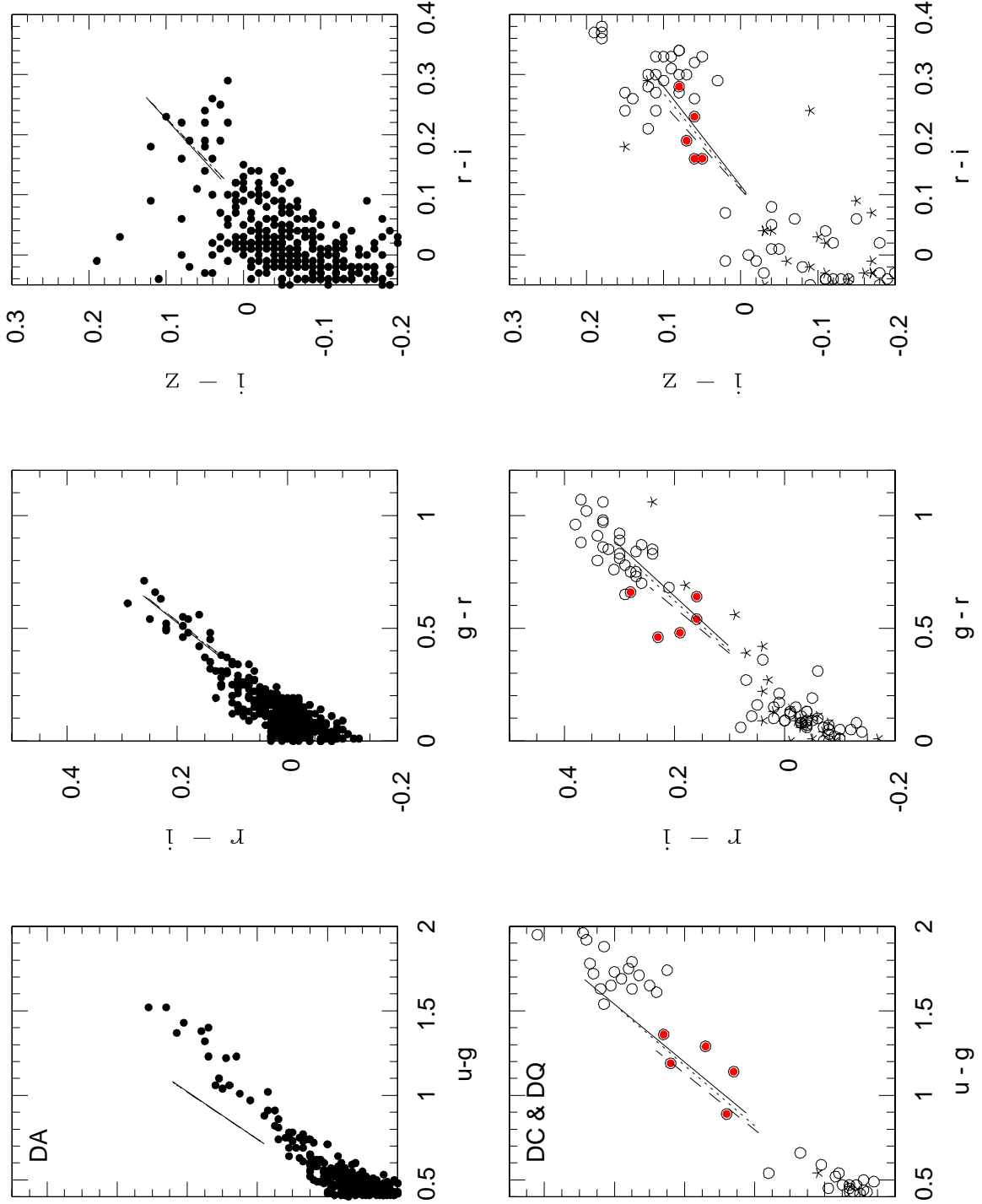


Fig. 10.— The  $u-g$  vs.  $g-r$  (left panel),  $g-r$  vs.  $r-i$  (middle panel), and  $r-i$  vs.  $i-z$  (right panel) color-color diagrams for white dwarfs in our sample. Upper panels show DA white dwarfs, whereas lower panels show DC (open circles) and DQ (star symbols) white dwarfs. The pure H (DA panels) and pure He (non-DA panels) model sequences with  $6000K \gtrsim T_{\text{eff}} \gtrsim 5000K$  are also shown for  $\log g = 7$  (solid line),  $\log g = 8$  (dashed line), and  $\log g = 9$  (dotted line). Probable DC white dwarfs in the non-DA gap are shown as filled red circles.

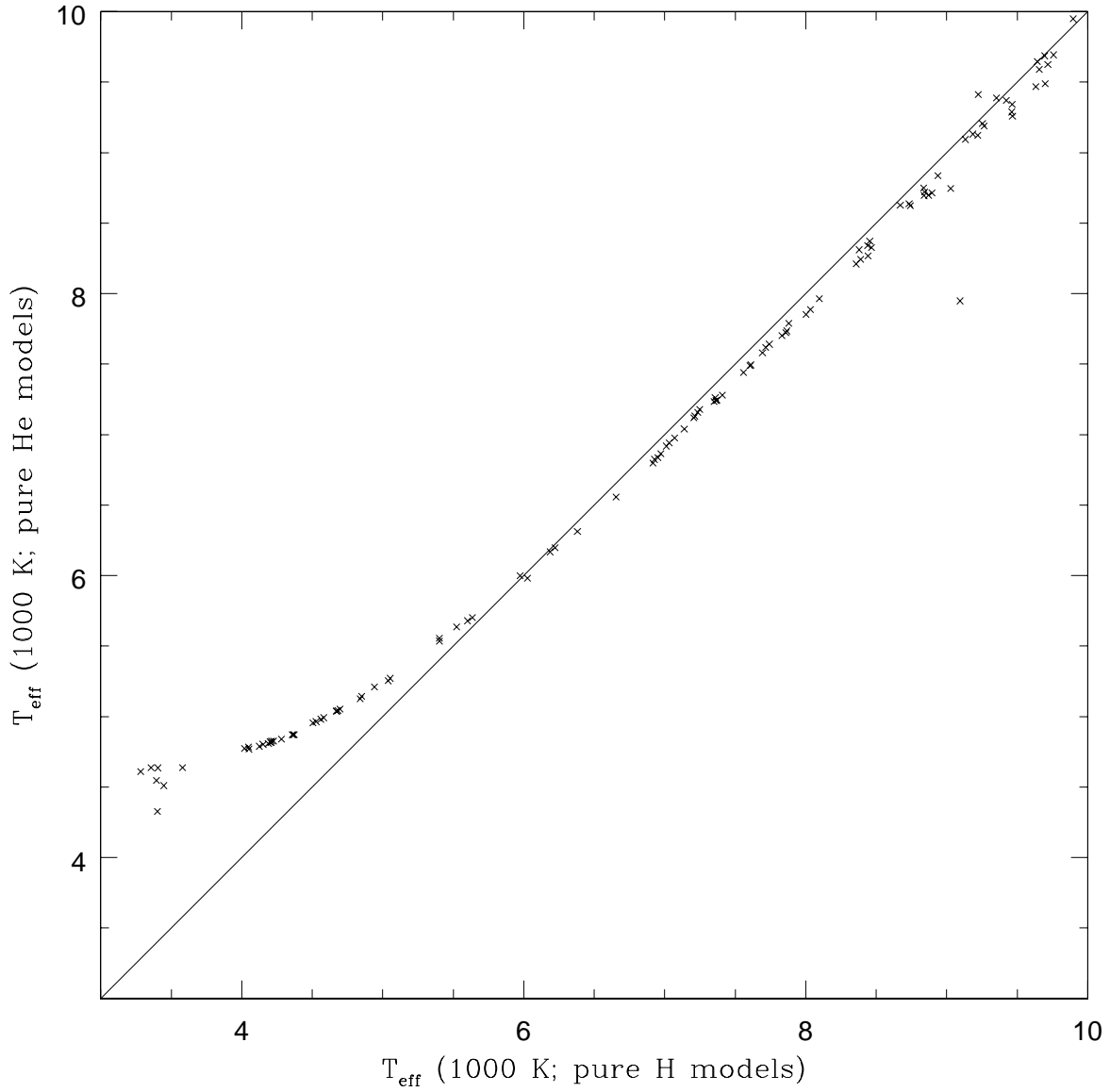


Fig. 11.— Effective temperatures for our sample of DC white dwarfs using pure H or pure He white dwarf model atmospheres. The effects of using a hydrogen-rich or a helium-rich composition to estimate temperatures become significant below  $\sim 5500K$ .